ABSTRACT

HUANG, TAI-YUN. Vibration of Thin Plates under Acoustic Excitations: its Application in Acoustic Metamaterials. (Under the direction of Dr. Yun Jing).

Over the past decade, a great amount of research efforts have been devoted to the topic of acoustic metamaterials (AMMs). The recent developments of AMMs have enlightened novel ways of manipulating sound waves due to the negativity of effective properties. Several potential applications, such as low-frequency noise reduction, cloaking, angular filtering, subwavelength imaging, and energy tunneling, have been proposed and implemented by the so-called "membrane- or plate-type AMMs without mass attached." This dissertation aims to present developed analytical/semi-analytical models for square/rectangular shaped membrane- or plate-type AMMs without mass attached, arbitrarily shaped AMMs without mass attached, and the heavy medium effect on the square/rectangular shaped plate-type AMMs without mass attached. These analytical/semi-analytical models can reveal the behind physics of structure and are powerful tools for designing AMMs. All derived models have been verified by the finite element method (FEM).

Vibration of Thin Plates under Acoustic Excitations: its Application in Acoustic Metamaterials

by
Tai-Yun Huang

A dissertation submitted to the Graduate Faculty of
North Carolina State University
In partial fulfillment of the
Requirements for the degree of
Doctor of Philosophy

Mechanical Engineering

Raleigh, North Carolina

2017

APPROVED BY:

_____	_____
Dr. Yun Jing Committee Chair	Dr. Fuh-Gwo Yuan
_____	_____
Dr. Richard Keltie	Dr. Yong Zhu

DEDICATION

To my parents, wife and friends with love

BIOGRAPHY

Tai-Yun Huang was born March 18, 1984, in Taiwan. He obtained his bachelor's degree in electrical engineering from the National Taipei University of Technology in 2006. After finishing mandatory military in Taiwan 2008, he came to the United States and obtained his master's degree in Physics from Pittsburg State University, Kansas, in 2011. In the fall of 2012, he came to North Carolina State University to pursue his PhD degree in Mechanical Engineering. His interests are acoustics, which include sound and plate-type structure interaction, plate-type structure vibration, and acoustic metamaterials design for noise reduction. He plans to obtain his PhD degree at the end of 2016. Outside of work, he likes to hang out with family and friends to chat, travel, and exercise. Playing basketball and ping pong are favorites.

ACKNOWLEDGEMENTS

Finding a research interest and direction was hard for me, especially after changing my major from physics to mechanical engineering in my first semester (fall 2012). Although I did not have much previous research experience in mechanical engineering, Dr. Yuan gave me the opportunity to stay in his group. I really appreciate Dr. Yuan's guidance in helping me find my research interests and strengths. Under Dr. Yuan's guidance, I took several useful courses (especially advanced structural vibration, which is taught by Dr. Keltie) and had the chance to read a paper about plate-type AMMs that lead me to take part in further research with Dr. Jing.

I am grateful for Dr. Jing, who gave me the opportunity to join his project and research. Without him, I could not have opened my mind and overcome all of the difficulties I met throughout the program. Despite the many clumsy questions I have asked Dr. Jing, he always shows enthusiasm in answering my questions. Under his patient guidance, I gradually have opened my mind and learned how to think by myself to accomplish research. With his recommendation, I had a chance to do a summer intern in Saint-Gobain, Massachusetts. This opportunity not only gave me working experience but also let me understand how the real world runs and how knowledge can improve current design. I am glad I met Dr. Shi, who is the acoustic group leader, and all my colleagues in Saint-Gobain. They gave me wonderful experiences and made me a mature person.

I really appreciate my parents give me a lot of support. Without them, I cannot have chance to do anything, i.e. live with happiness and study aboard to pursue my dream. Although sometimes we had different opinions, we still love with each other. Thank you,

my parents, very much for your great patience. My wife, Betty, she is a beautiful, wise and gritty girl. Because of her, I have courage to open my mind and am able to walk further in faith each day. I really appreciate your fully love which always supports me. For all I met in my surrounding, i.e. Professors and classmates from courses, colleagues from lab, teammates from basketball court and friends from my life, I really appreciate all of your accompany and support. You bring me happiness.

TABLE OF CONTENTS

LIST OF FIGURES

Chapter I

Introduction

1.1 Motivation

In recent years, metamaterials have drawn a lot of attention in the scientific community due to their unusual properties and useful applications. Metamaterials are artificial materials made of subwavelength microstructures. They are well known to exhibit exotic properties and manipulate wave propagation in a way nature materials cannot. Metamaterials were first considered from the idea of simultaneously negative dielectric constant (ε) and magnetic permeability (μ) for Electromagnetic (EM) waves [7]. Later on, John Pendry presented the first man-made structure to achieve negative permeability and also showed that the negative refractive could be fulfilled by a periodic structure [8]. These two seminal papers opened up a new field and have driven a vast amount of research on EM metamaterials, such as breaking the diffraction limitation for imaging [9], cloaking EM waves [10], and ultra-broadband light absorption [11].

The idea of creating acoustic metamaterials (AMMs) [12][13][14] and elastic wave metamaterials [15]–[17] follows that of EM metamaterials, thanks to concept analogy. AMMs have drawn a lot of attentions in recent years since their unique effective material properties can lead to extraordinary abilities for manipulating wave propagation [14][18][19]. Liu *et al.* pioneered the realization of locally resonant AMMs, which consist of a dense core with a soft elastic coating, both embedded in a matrix material [20]. This sonic crystal structure behaves as an effective medium with negative effective

density and can fully reflect normal incident sound waves within a certain frequency range.

Following the idea of locally resonant AMM, Yang *et al*. demonstrated the first membrane-type AMMs with mass attached [21]. Negative effective density, however, can only be achieved within a narrow frequency band. Near-total reflection can be achieved at a frequency between the first two eigenmodes of the membrane. Several similar works [22][23][24][25]were carried out to tune the negative effective density and create broadband sound insulation by using different masses on the same or different stacked membranes.

Shortly after ref. [21] was published, Lee *et al.* proposed a low-loss, membrane-type AMMs without mass attached [26]. Multiple stretched and fixed membranes were placed with a certain separation distance in a waveguide. Broadband negative density was observed below the first resonance frequency of the membrane. One potential problem of the membrane-type AMM without mass attached is that it relies on the tension of the membrane, which is difficult to control and sustain over a period of time. To cope with this problem, plate-type AMMs without mass attached were proposed [27]. The vibration of the plate depends on the elastic properties of the plate material and is therefore much easier to control [19][28][29].

The broadband sound insulation effect was experimentally demonstrated using a lightweight thin-plate AMM without mass attached that could yield sound transmission loss (STL) consistently higher than 45 dB below 500 Hz [30]. Shen *et al.* designed a complimentary metamaterial (CMM) in which the effective density can be tuned to a

certain value in order to perfectly cancel out the unwanted aberrating layer [5]. Plate-type AMMs without mass attached can provide a smooth transition for effective density from negative values to positive values so that near-zero effective density arises [1]. This can lead to several applications, including subwavelength imaging [31][32], cloaking [33], angular filtering [34], and energy tunneling [35].

As the result of the many advantages of plate-type AMMs without mass attached, e.g. relatively easy control of the material and broadband negative effective density, a large amount of work has been carried out. Some of this research was mentioned in the previous paragraph. Other relevant works can be found in a recent review paper [19]. To facilitate the design of the plate-type (or membrane-type) AMMs without mass attached (hereinafter, if not mentioned in Chapters III -VI, the plate-type AMMs referred to are those without mass attached) for various applications, it is crucial to develop an accurate, yet robust, method to evaluate the effective density of these AMMs. This is important point for AMM designs [5].

1.2 Objective

The objective of this dissertation is to develop analytical models for evaluating the effective density of a plate-type (or membrane-type) AMM under different situations, that is, (1) plate- and membrane-type AMMs with square-shaped plates and membranes (as a benchmark of derivation); (2) plate-type AMMs with arbitrarily shaped plates; and (3) plate-type AMMs considering the fluid effect.

1.3 Outline

Chapter I explains the motivation and objectives of this research. A thorough overview of the recent developments in membrane- or plate-type AMMs is provided in Chapter II. The underlying mechanism of these types of AMMs for tuning the effective density will be first examined. Four different groups of membrane- or plate-type AMMs (membranes with masses attached, plates with masses attached, membranes or plates without masses attached, and active AMMs) will be reviewed. The opportunities for, limitations of, and challenges of membrane- or plate-type AMMs also will be discussed.

The effective densities of plate- and membrane-type AMMs without mass attached are theoretically and numerically studied in Chapter III. Three models, including the analytic model (based on the plate flexural wave equation and the membrane wave equation), approximate model (under the low frequency approximation), and FEM model, are first used to calculate the acoustic impedance of square and clamped plates or membranes. The effective density is then obtained using the resultant acoustic impedance and a lumped model. Pressure transmission coefficients for the AMMs are computed using the obtained densities. The effect of the loss from the plate also is taken into account. Results from different models are compared, and good agreement is particularly found between the analytic model and the FEM model. The approximate model is less accurate when the frequency of interest is above the first resonance frequency of the plate or the membrane. The approximate model, however, provides simple formulae to predict the effective densities of plate- or membrane-type AMMs and is accurate for the negative density frequency region.

The effective densities of arbitrarily shaped plate-type AMMs without mass attached are studied in Chapter IV. Acoustic impedances of three different shaped plates, i.e. circle, triangle, and hexagon, are calculated by the meshless boundary method and the effective densities are calculated using the lumped model. To validate the accuracy of this framework, the numerical results are compared with the analytical solution as well as the finite element method (FEM) for circular plates and are compared with FEM for the other two shapes. In general, good agreements can be found provided that a sufficient number of edge points and collocation points are used in the meshless boundary method. Notably, for the triangular shape, some discrepancies are found at the low-frequency region, and this might have been because of the sharp corners of the triangle.

The effective densities of plate-type AMMs with considering fluid effect are studied. The analytical model is developed in Chapter V. Because of the fluid effect, the reaction pressure from fluid medium is obtained by the waveguide theory and then included in the analytical framework. Results show that for a light fluid medium, i.e. air, the fluid effect can be ignored, but for a heavy fluid medium, that is, water, the fluid effect is significant and can’t be ignored.

The main conclusions and future work are presented in Chapter VI.

Chapter II

Background

The very first approach of AMMs utilized composite materials composed of lead balls, epoxy, and rubber [12][36]. Negative density can be induced by the local-resonance of this structure. Since then, other novel AMMs have emerged in this area, such as perforated plate type AMMs [37][38] and space-coiling type AMMs [39]–[44]. In this chapter, a specific type of AMMs, i.e., the membrane- and plate-type AMMs, will be reviewed. Compared with other AMMs, this type of AMMs is in general light-weight, which is particularly important for noise control. They also have relatively simple geometries and the ability to actively tune the effective density. Most importantly and uniquely, a broad-band negative effective density can be observed with very low loss [45] if properly designed. Thus, they have generated a large interest in the AMM community to explore their theory, mechanism and applications. A variety of designs based on the membrane- and plate-type AMMs have been proposed and implemented to explore and expand their applications. Four different groups of membrane- and plate-type AMMs will be discussed and they are as follows: membranes with masses attached, plates with masses attached, membranes or plates without masses attached, and active AMMs. These AMMs have found applications in low-frequency sound attenuation [26][27][30], cloaking [33], angular filtering [34], subwavelength imaging [31][32], energy tunneling [35], etc. Unlike membrane-type AMMs which mainly manipulate the transmission, reflection, and absorption of acoustic waves, plates with attached masses could control either the acoustic waves interacting with them or elastic waves propagating within the plates (e.g., flexural and lamb waves). For instance, attaching a 2D array of composite

stubs [46]–[50] on the surface of a thin plate could manipulate the plate's lamb modes. This chapter, however, focuses on the plate-type AMMs for manipulating acoustic waves.

2.1 Effective density of membrane- and plate-type AMMs

To begin, it is useful and important to understand the mechanism of membrane- and plate-type AMMs for tuning the effective density. Two simple yet representative examples are illustrated in Figs. 2.1(a) and (b), where a membrane or a thin plate is clamped inside a subwavelength waveguide, with or without a mass attached, under the excitation of plane waves. When the membrane (plate) vibrates under the acoustic excitation, the effective/dynamic density arises due to the restoring force associated with this structure, as will be detailed below. These AMMs have been adopted in [1][3][26] and many other papers that will be reviewed here.

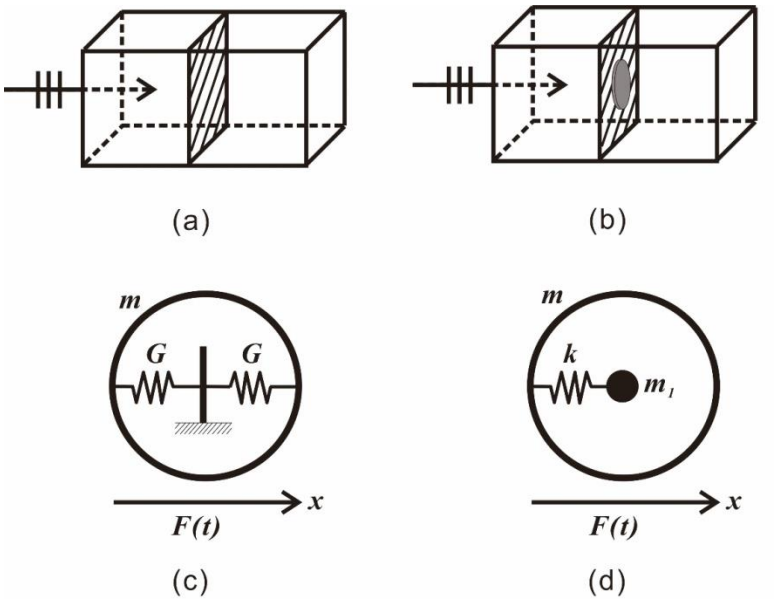

Figure 2.1. A membrane or plate clamped in a waveguide. (a) Without mass attached. (b) With mass attached. (c) The corresponding mass-spring diagram for (a). (d) The corresponding mass-spring diagram for (b).

We first discuss the case without masses attached on the membrane or plate (Fig. 2.1(a)). For a vibrational thin plate under acoustic excitation, the governing equation can be written as

$$D\nabla^4 W(x,y,t) + \rho h \frac{\partial^2 W(x,y,t)}{\partial t^2} = P(x,y,t) \tag{2.1}$$

where x and y are the spatial coordinates on the plate; t is time ; D is the flexural rigidity and $D = Eh^3/12(1-\nu^2)$; P is the external pressure; E , ν , ρ and h are the Young's Modulus, Poisson's ratio, density and thickness of the plate, respectively.

For a vibrational membrane under acoustic excitation, the governing equation reads

$$T\nabla^2 W_1(x,y,t) - \rho_1 h_1 \frac{\partial^2 W_1(x,y,t)}{\partial t^2} = -P_1(x,y,t) \tag{2.2}$$

where T is the uniform tension per unit length; P_1 is the external pressure; ρ_1 and h_1 are the density and thickness of the membrane, respectively. As can be seen from Eqs (2.1) and (2.2), In general, the vibrational response of a membrane is intrinsically dictated by the tension applied whereas the vibrational response of a thin plate is dominated by its stiffness. This distinguishes the membrane-type AMMs from the plate-type AMMs (although in many occasions, the word "membrane" has been used to describe a thin plate [5][31][32]). Equations (2.1) and (2.2) can be solved either numerically or analytically (e.g., for a circular thin plate) and the effective density can be estimated for the AMM. For example, the transverse displacement and acceleration could be obtained and the effective mass density could be calculated by

$$\rho_{eff} = (\bar{p}_1 - \bar{p}_2)/\bar{a}_z , \tag{2.3}$$

where $\bar{p}_1$ and $\bar{p}_2$ are the surface integrations of pressures over the left and right surfaces, respectively, of the membrane or plate and $\bar{a}_z$ is the volume integration of the normal acceleration of the membrane or plate. For the AMM shown in Fig. 2.1(a), the effective density has been shown to follow the Drude form and could be written as [26]

$$\rho_{eff} = \rho' \left(1 - \frac{\omega_c^{\,2}}{\omega^2} \right), \tag{2.4}$$

where ρ' is the average density of the air loaded with the membrane or plate and ω_c is the first resonance frequency of the membrane or plate. We note that Eq. (2.4) has only been proved valid for air. For other fluids, such as water, the effect of the fluid loading on the membrane or plate is much stronger and Eq. (2.4) may possibly need to be revised. Clearly, at a frequency below the first resonance frequency, the effective density is negative, therefore resulting in a broadband negative density AMM. Within this frequency range, the acceleration of the membrane or plate is found to be out-of-phase with respect to the external excitation [26]. Close to the resonance frequency, the effective density is near-zero. A figure showing the effective density of a clamped, thin plate can be found in Fig. 2.2. Alternatively, the effective density of this AMM can be understood by a mass-spring system as shown in Fig. 2.1(c) [51]. In the system, a mass *m* is confined by two springs *G* fixed to the ground. The effective mass of a 1-D lattice system composed of this unit cell reads

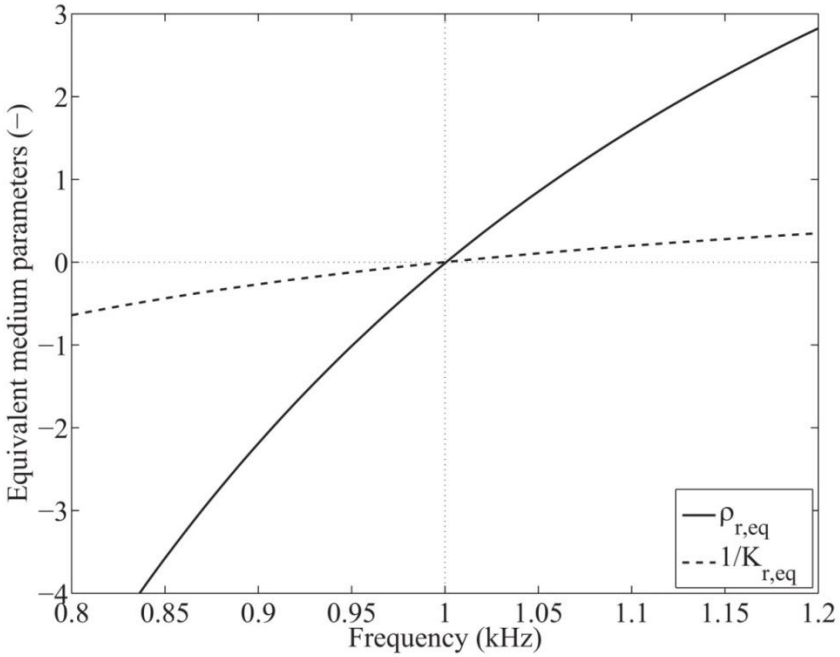

Figure 2.2. The normalized effective density (solid line) and bulk modulus (dashed line) of a thin plate-type AMM with open channels. Taken from Bongard *et al.* [1].

$$m_{eff} = m\left(1-\frac{\omega_0{}^2}{\omega^2}\right), \tag{2.5}$$

where $\omega_0 = \sqrt{\frac{2G}{m}}$. Equation (2.5) is in the same form with Eq. (2.4). In the membrane- or plate-type AMM, the membrane or plate behaves as the springs and the masses. They are clamped on the boundaries just as the springs are fixed to the ground.

For the membrane- or plate-type AMMs with mass attached shown in Fig. 2.1(b), the vibrational governing equations become more complicated. For example, for a membrane with a mass attached, the governing equation reads [52]

$$\rho_1 h_1 \frac{\partial^2 W_1(x,y,t)}{\partial t^2} - T\nabla^2 W_1(x,y,t) = p_1 - p_2 + \sum_{i=1}^{I} Q_i(t)\delta(x-x_i)\delta(y-y_i), \tag{2.6}$$

where $p_1 - p_2$ is the net acoustic pressure applied on the membrane and the third term on the right hand side of the equation is the summation of point forces (Q_i) at collocation points (I) on the interface between the membrane and mass; δ is the Dirac delta function.

For a plate with multiple masses attached, the governing equation can be written as [53]

$$D'\nabla^4 W(x,y,t) - T\nabla^2 W(x,y,t) + \rho h \frac{\partial^2 W(x,y,t)}{\partial t^2} = p_1 - p_2 + \sum_{s=1}^{S}\sum_{i=1}^{I} F_i^{(s)} \delta\left(x - x_i^{(s)}\right)\delta\left(y - y_i^{(s)}\right) \tag{2.7}$$

where $D' = D + \frac{\sigma_0 h^3}{12}$ is the effective bending stiffness, σ_0 is the initial stress on the plate; the inner summation (*i*) is similar to the summation in Eq. (2.6); the outer summation (*s*) accounts for multiple masses attached at different positions on the plate. Compared with Eq. (2.1) for plates, Eq. (2.7) includes the initial tension term (the 2nd term on the left hand side of the equation) and therefore is more generic.

Similarly, these governing equations can be solved and the effective density can be evaluated by using Eq. (2.3) or other approaches. In contrast to the membrane- or plate-type AMMs without mass attached, where deep/large negative density could occur within a broadband frequency, the addition of the mass introduces a resonance-based, relatively narrow frequency band negative density. For example, Yang *et al*. [3] observed that deep negative density occurs around the anti-resonance frequency, i.e., a frequency between the first and second resonance frequencies of the membrane with a mass attached. The corresponding effective density is shown in Fig. 2.3 [2]. A mass-spring system has also been established to understand this resonance-based negative density. As can be seen in

Fig. 2.1(d), an inner mass m_1 is connected to an outer mass m through a spring k and the effective mass can be written as [54]

$$m_{eff}' = m + \frac{m_1 \omega_0^2}{\omega_0^2 - \omega^2}, \tag{2.8}$$

where $\omega_0 = \sqrt{\frac{k}{m_1}}$. In the absence of loss, this effective mass is in the Lorentz form.

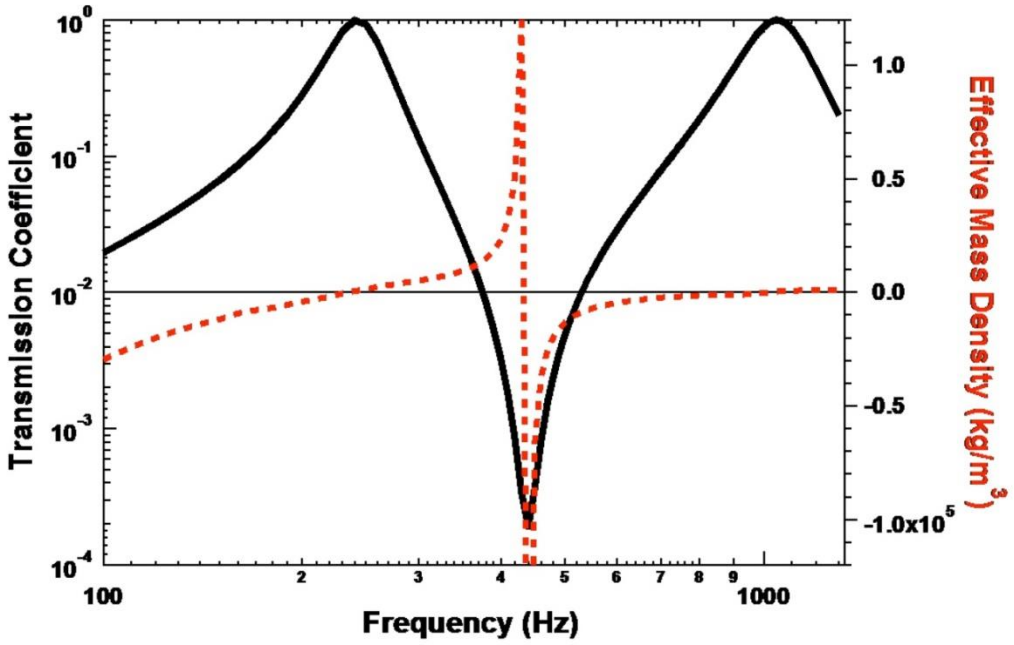

Figure 2.3. (Color online) The transmission coefficient (solid line), which is the ratio of the magnitude of the transmitted pressure to the magnitude of the incident pressure, and effective mass density (dashed line) of a membrane-type AMM with mass attached are shown. The negative effective mass density occurs below the first resonance frequency (231 Hz) and the region between the anti-resonance frequency (448 Hz) and the second resonance frequency (1053 Hz). Taken from Ma [2].

2.2 Different designs of membrane- and plate-type AMMs and their potential applications

2.2.1 Membrane-type AMMs with masses attached

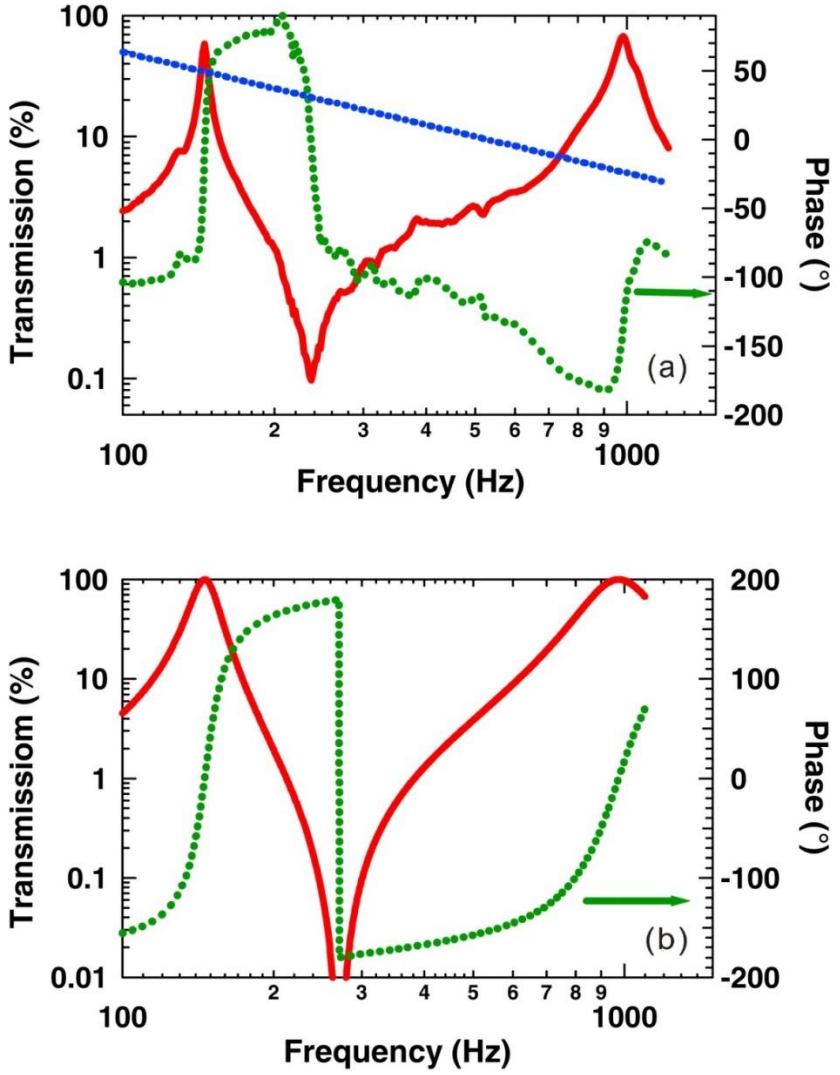

Figure 2.4. (Color online) The sound transmission (ratio of the magnitude of the transmitted pressure to the magnitude of the incident pressure in percentage) and the phase of a membrane-type AMM with mass attached are shown. (a) Experimental result. Solid line is the transmission and the dotted line is the phase. The straight dotted line shows the mass law. (b) Numerical result. Solid line is the transmission and the dotted line is the phase. The two resonance frequencies are 146 Hz and 974 Hz where the transmission peaks occur. The anti-resonance frequency is 272 Hz where the transmission dip occurs. Taken from Yang *et al*. [3].

Yang *et al*. [3] demonstrated the first membrane-type AMMs (similar to that shown in Fig. 2.1(b)). It was found that a stretched membrane with different masses attached could produce different vibrational modes with corresponding different transmission behaviors. In general, two peaks and one dip in between can be observed in the sound transmission curve below the 2^{nd} resonance frequency. While the peaks were caused by the two eigenmodes, the dip was due to the anti-resonance (both eigenmodes are excited but with opposite phase). At the two eigenmode frequencies, the average displacements on the membrane were relatively large, leading to high transmission. At the transmission dip frequency, the average displacement was minimum, which was responsible for the low sound transmission and large sound reflection. The extremely low sound transmission at this very low frequency was found to break the well-known mass law (Fig. 2.4). By tuning the mass attached on the membrane, the transmission curve can be tailored. For instance, by increasing the weight of the mass, the two peaks will shift to lower frequencies.

Later on, Yang *et al.* [23] extended their work to an array of membrane with attached masses which could be used for light-weight low-frequency sound reduction. Furthermore, to achieve broadband sound reduction, several AMM panels with different mass weights were stacked up. An average sound transmission loss (STL) > 40 dB was achieved over the 50-1000 Hz frequency range with stacked panels thinner than 60 mm and lighter than 15 kg/m^2. The STL of this type of AMMs was further investigated numerically and experimentally by Naify *et al.* [24] by varying the mass and tension on the membrane. The corresponding out-of-plane displacement of the membrane was measured by a laser vibrometer. Naify *et al.* [22] later changed the geometry of the

attached masses to coaxial rings. Samples with different number of rings and distribution of masses were tested both numerically and experimentally. In comparison with the previous studies where the mass weights are placed at the center of the membranes, either the bandwidth of the STL peak was broader or multiple STL peaks could arise. Shortly after, the same group attempted to arrange multiple membrane-type AMMs with masses in a rectangular array to address the scale-up issue of this structures [25]. Multiple arrays were also stacked up to examine the interaction between the layers and improve the STL [55]. In the case of different masses involved, multiple STL peaks occurred correspondingly.

Similar to [25], Zhang *et al.* [56] also investigated membrane-type AMMs with different or identical attached masses. It was claimed that for membranes carrying different masses, the low-frequency STL can be improved. Zhang *et al.* [57] presented a theoretical model for the membrane-type AMM with a single mass. The inertia force of the mass was treated externally as a concentrated force in the governing equation of the membrane. By applying a normal incident sound wave on the AMM, the STL could be obtained analytically. The effect of varying the position of the mass was also studied and the frequency shift was found to be not significant.

Chen *et al.* [52] developed the theoretical model for circular membrane-type AMMs with multiple, arbitrarily shaped masses. Langfeldt *et al.* [58] also established an analytical model for both circular and rectangular membrane-type AMMs with masses in arbitrary shape. Tian *et al.* [59] introduced a theoretical model for circular membrane-type AMMs with attached rings. Similar to [11], the inertia force of the ring mass was treated as a concentrated force on the membrane. When the inner radius of the ring

increased with a constant weight, the resonance frequencies were found to become higher. The same phenomenon can be also achieved by decreasing the weight of the ring. When multiple rings with different inner radii are present, multiple resonance frequencies can be observed.

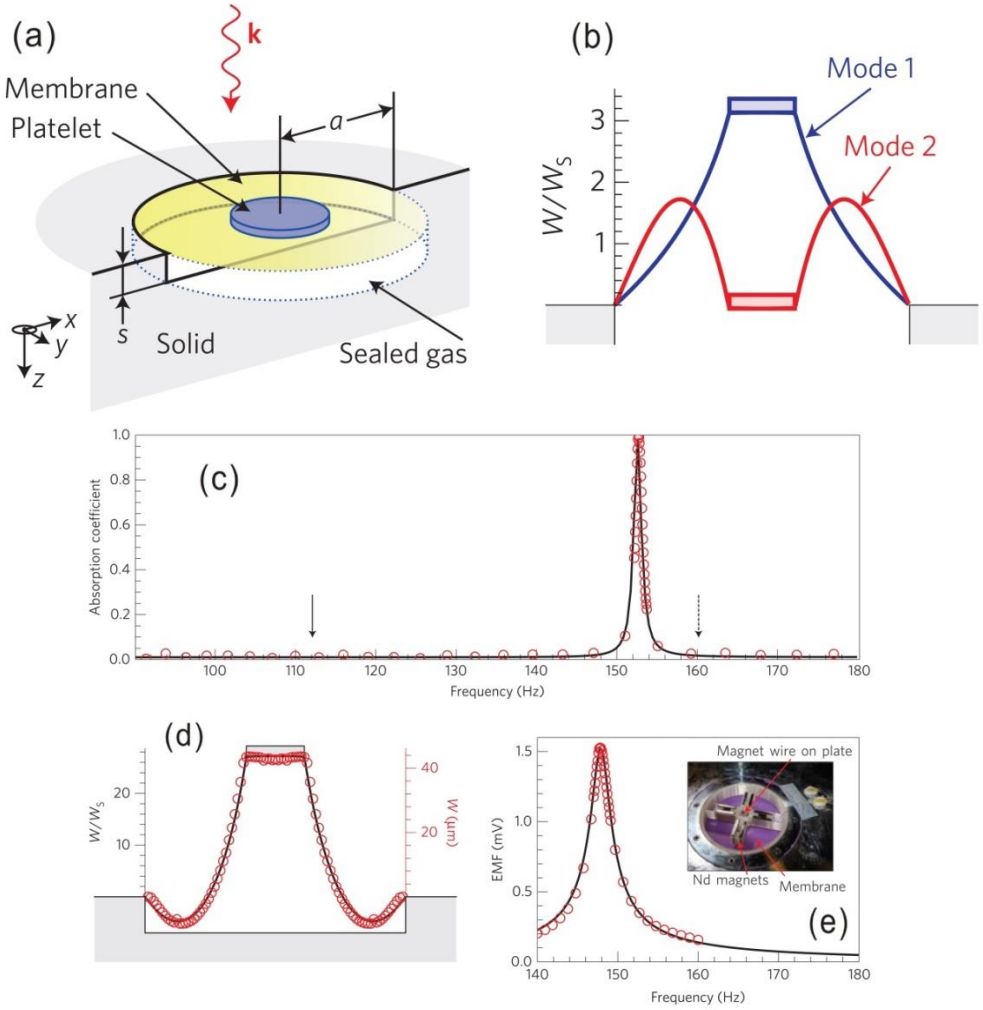

Figure 2.5. (Color online) The ultrathin membrane-type AMM (metasurface) for super-absorption. (a) The schematic of the structure. (b) The out-of-plane displacements of the two lowest eigenmodes of the membrane with mass attached. (c) The theoretical (solid line) and experimental (circles) absorption curves. The solid and dashed arrows indicate the first resonance frequency and anti-resonance frequency, respectively. The absorption coefficient is defined by the ratio of the absorbed sound energy to the incident sound energy. (d) The out-of-plane displacements at the absorption peak frequency. (e) The electromotive force (EMF) generated by the vibration of the AMM. The inset shows the experimental set-up. Taken from Ma *et al.* [4].

Mei *et al.* [60] proposed a different type of membrane-type AMMs (the so-called dark acoustic metamaterials) which could yield almost 100% acoustic absorption at very low frequencies within a narrow band as demonstrated by their experiments. The proposed AMMs consist of fixed rectangular membranes decorated with semi-circular iron platelets, backed with an aluminum reflector. The underlying mechanism of this dark AMM is that at resonance frequencies, acoustic energy is converted into elastic energy through flapping motion of the platelets and then dissipated efficiently. The resonance frequencies where peak absorption occurs can be tuned by adjusting the weight of the platelet or the separation between two platelets: reducing the lower absorbing frequencies by increasing the weights of platelets; decreasing the higher absorbing frequencies by increasing the separation of platelets.

Chen *et al.* [53] theoretically analyzed the dark AMM under a plane normal incidence by using the modal expansion and point matching methods. The acoustic absorption coefficient can be accurately predicted and microstructure effects were also considered. Ma *et al.* [4] introduced another ultrathin membrane-type AMM (the so-called metasurface) for super-absorption at certain tunable frequencies (Fig. 2.5). This AMM is comprised of a circular membrane attached with a platelet at the center. The membrane is mounted over a solid surface with sealed gas in between. The reason for the full absorption is that the AMM surface becomes impedance-matched to air at certain frequencies due to hybrid resonances. It was also demonstrated that a high acoustic-electrical energy conversion efficiency of 23% can be achieved using a setup consisting of magnet wires and magnets. Yang *et al*. [61] presented a generalized perspective for understanding the sound absorption and scattering of the membrane-type AMM with

masses attached and also experimentally demonstrated perfect sound absorbers based on degenerate decorated membrane resonators [62].

In contrast to most membrane-type AMMs which only induce negative effective density, Yang *et al.* [63] proposed a membrane-type AMM that could exhibit both negative effective density and negative effective bulk modulus in a relatively broadband frequency range. This device has two membranes (top and bottom) each with a rigid disk attached. The two membranes are connected by a plastic ring and are fixed to a side wall. Two types of resonance modes could be produced by this structure, i.e. the monopolar and dipolar resonances. Under the monopolar resonance, the two disks vibrate out-of-phase and the ring is motionless. Under the dipolar resonance, the two disks vibrate in phase. The ring vibrates either in phase or out-of-phase with respect to the two disks. The monopolar resonance is responsible for the negative effective bulk modulus whereas the dipolar resonance creates the negative effective density. Within the frequency range where monopolar and dipolar resonances overlap, double negativity could be achieved.

Recently, Ma *et al.* [64] fabricated and tested a purely flexible membrane-type AMM. Although the structure looks similar to that in [3], all materials used are lightweight and flexible, which could be advantageous in practice.

Ma *et al.* [65] designed a membrane-type AMM consisting of four fully clamped membranes with attached disks. A sizable orifice was situated at the center of the material. While this design allows air flow and heat exchange through the orifice, it also yields high STL in a low-frequency narrow bandwidth. It was found that interaction of resonating field of the AMMs with the sound field passing through the orifice is responsible for the large STL.

2.2.2 Plates with masses attached

It has been found that masses attached on plates could also give rise to many intriguing phenomena. Xiao *et al.* [66] theoretically studied the STL through an unbounded thin plate with spring-mass resonators (SMRs) attached using the plane wave expansion method and effective medium method. The STL of the diffuse sound field was obtained by first solving for the STL at different incident angles. The authors showed that using an extremely thin plate could lead to high STL at low frequencies. Li *et al.* [67] studied multiple layers of thin plate-type AMMs with SMRs attached using the transfer matrix method. Their paper, however, focused more on the effective density of this AMM. Under normal incidence plane wave, they found that the effective density could follow either the Loerntz-form or Drude-form model. For oblique angles, the effective density depends on the lateral wave number of the incident wave.

The STL for thick plates with SMRs was obtained theoretically by Oudich *et al.* [68]. Unlike the theoretical model in Xiao's paper [66] which only considered flexural waves, a more general case taking other types of elastic waves into account was considered using the plane wave expansion method. Gusev *et al.* [69] applied the analytical lumped-element approach to study a double negative meta-plate which exhibited both effective negative density and negative bending modulus for flexural waves. The effective negative density was introduced by normal-force interactions in the resonators vertically attached on the plate. The effective negative bending modulus was achieved by the lateral forces and rotational inertia interactions due to the resonators horizontally attached on the plate.

2.2.3 Membrane- or plate-type AMMs without masses attached

For membrane-type AMMs with mass attached, deep effective negative density in general can only be acquired within a narrow frequency band. In addition, since the negative density is primarily due to resonances, energy loss could become a critical issue. To overcome these limitations, Lee *et al.* [26] proposed a low-loss, membrane-type AMMs without mass attached. They placed multiple stretched membranes with a certain separation distance in a waveguide. The edges of the membrane were fixed. The tension on the membrane was calibrated by applying water weight and observing the deformation of the membrane. Negative density was observed below the first resonance frequency of the membrane and the Drude-form effective density was theoretically derived, i.e., Eq. (2.4). Shortly after, the same group combined this membrane-type AMM with branch openings (side holes) to achieve double negativity [70], since branch openings can introduce negative bulk modulus [71][72]. A sample was fabricated and tested. The phase velocity was found to be negative under the cutoff frequency of the branch opening f_{SH} and reversed Doppler effect can be observed [73]. Above the resonance frequency (f_c) of the membrane, the AMM is double positive. At a frequency between f_{SH} and f_c, the AMM is single negative (only the effective density is negative). Fan *et al*. [74] theoretically and experimentally studied nonlinear wave propagation in this specific type of AMM. The sound pressure amplitude was found to affect the pass and forbidden bands due to the nonlinear effect. This, however, could create opportunities for automatically triggered acoustic isolators and tunable acoustic metamaterials.

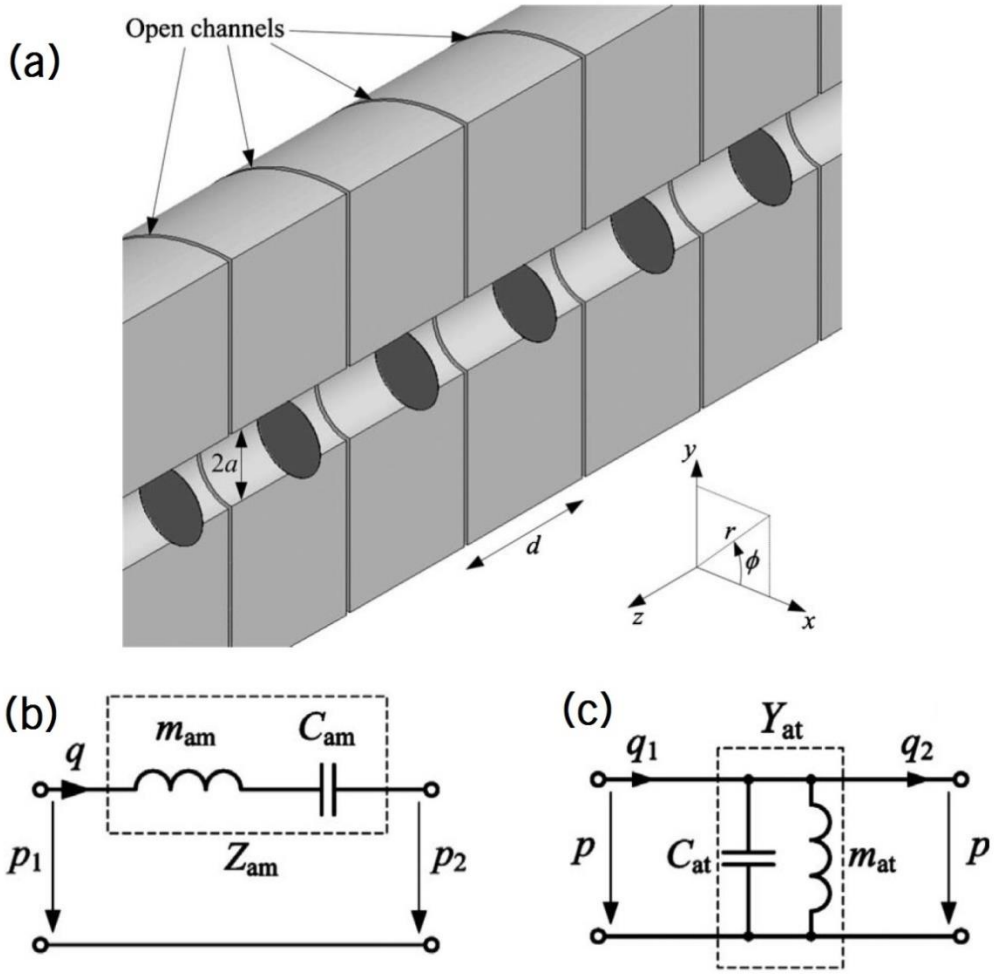

Figure 2.6. A plate-type AMM without mass and with radial open channels. (a) The cutaway view of the AMM. (b) The equivalent acoustic circuit for a membrane clamped in the waveguide. The acoustic impedance (Z_{am}) of the membrane consists of an acoustic mass (m_{am}) and compliance (C_{am}) in series. (c) The equivalent acoustic circuit for an open channel. The acoustic admittance Y_{at} consists of an acoustic mass m_{at} and compliance C_{at} in shunt. Taken from Bongard *et al.* [1].

Bongard *et al.* [1] investigated plate-type AMMs without mass attached (Fig. 2.6). The acoustic impedance of thin plates was first analytically derived. The transmission line approach was then used to estimate the relevant acoustic parameters, including the transmission, phase, and effective medium parameters. Similar to [24], the effective

density was found to be negative below the first resonance frequency of the thin plate. In addition, open channels were adopted to introduce negative bulk modulus. The refractive index can be therefore tuned from negative to zero and to positive. A possible application on directive acoustic sensor (acoustic leaky-wave antenna) was suggested in this paper and was later experimentally validated by Naify *et al*. [75]. Meanwhile, Yao *et al.* [51] attempted to use a spring-mass lattice system to explain the negative density below the cut-off frequency. As an example, an elastic 1-D waveguide (very thick plate) with clamped boundaries was demonstrated numerically. An array of elastic plates were also fabricated and tested for the sound transmission to show the noise reduction performance in the low frequency region.

Fan *et al.* [76][77] theoretically studied the 1-D circular membrane-type AMM with or without branch openings using the fluid impedance theory and Bloch theory to obtain the transmission and dispersion curves. Park *et al.* [45] constructed a 2-D membrane-type AMM for amplification of evanescent waves. Such a phenomenon was possible due to the negative effective density resulted from the membranes-type AMM [78]. Potential applications include acoustic superlensing, which was demonstrated recently that showed a resolution at 1/17 of the wavelength thanks to the surface wave stemming from the negative density [79]. Inspired by the electromagnetic wave complementary metamaterials (CMM), Shen *et al.* [5] designed a quasi-2-D acoustic CMM using acoustic coordinate transformation (Fig. 2.7). It was demonstrated that anisotropic, negative density as well as negative bulk modulus required for the acoustic CMMs can be achieved via plate-type AMMs (although the word “membrane” was used in the paper to describe the thin plate) with branch openings. To create anisotropic effective density, the

thin plates facing x- and y-directions were designed to have different thicknesses. The acoustic CMM was numerically demonstrated to be able to enhance the sound transmission through aberrating layers and reduce the sound field distortion. Such a CMM could allow better sound transmission through the human skull to enable transcranial brain imaging. Most recently, a similar AMM with anisotropic density was proposed to achieve hyperbolic dispersion [29].

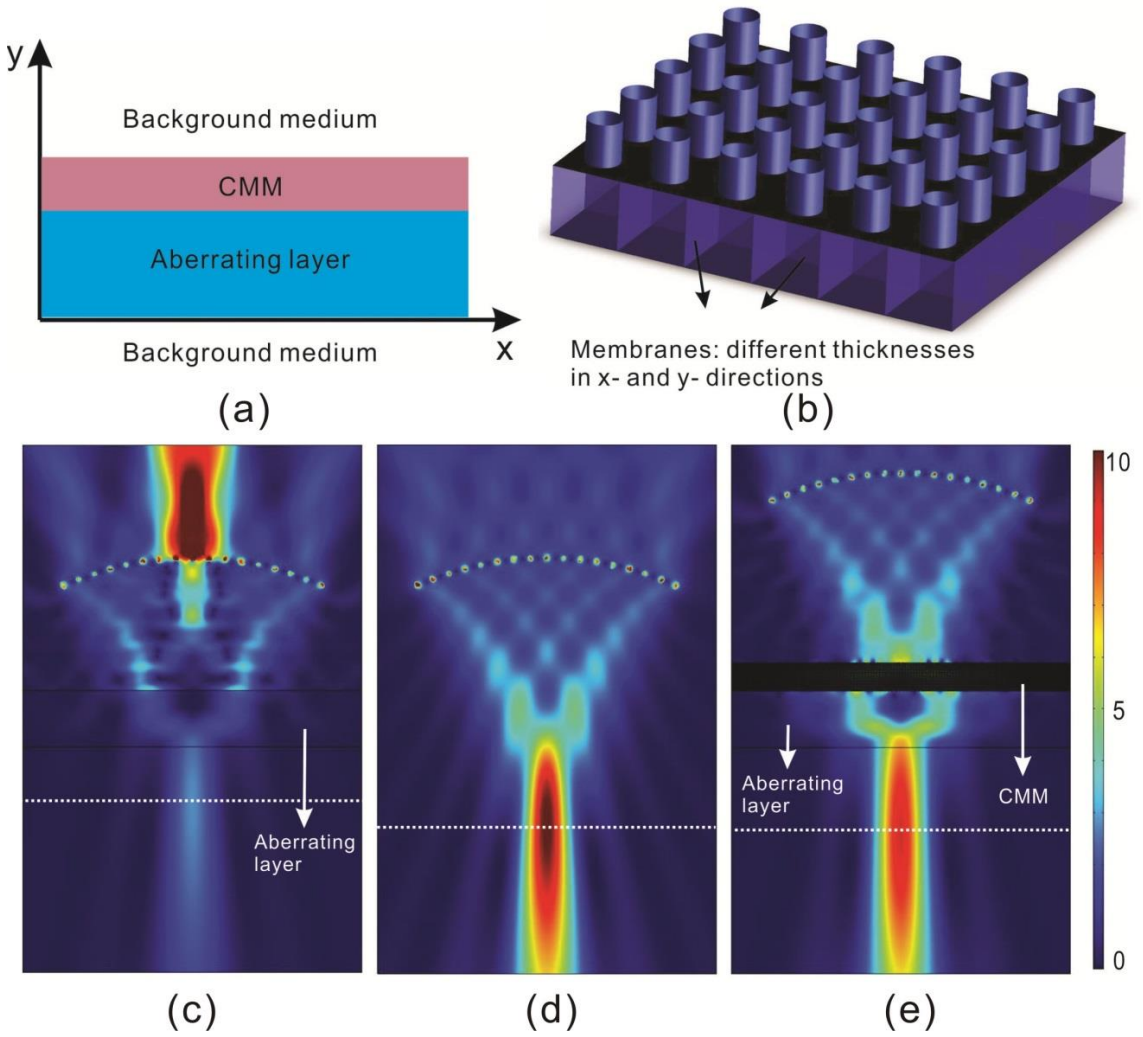

Figure 2.7. (Color online) The quasi-2-D acoustic CMM. (a) The CMM layer is used to acoustically cancel out the aberrating layer beneath it and to allow better sound transmission. (b) Schematic of the 2-D CMM layer. (c) The acoustic intensity field (W/m^2) of a focused beam with the aberrating layer only (human skull). (d) The acoustic intensity field (W/m^2) of a focused beam in a homogeneous medium (water). (e) The acoustic intensity field (W/m^2) of a focused beam with both the CMM layer and the aberrating layer. The sound energy transmitted through the aberrating is significantly strengthened thanks to the CMM. Taken from Shen *et al.* [5].

A number of work have been carried out utilizing membrane- or plate-type AMMs for showcasing density near-zero metamaterials (near-zero density typically occurs around the first resonance frequency of the membrane or plate). It was theoretically

predicted that [31][80] superlensing can be achieved by using an AMM with anisotropic density: density being near zero in one direction and infinite in another. A superlensing device was designed based on this idea using the plate-type AMM [80]. The authors also pointed out that at the near-zero frequency, all plates in parallel vibrate in phase, giving rise to the uniform phase in the density near-zero AMM. This superlensing effect was recently verified experimentally [32]. The plate material was paper, which has a relatively low energy loss. A resolution of 0.16 wavelength was demonstrated. Jing *et al*. [34] numerically demonstrated that when a 2D array of plate-type AMMs operate at the density near-zero frequency, only near-normal incident waves can transmit through the AMM, leading to an angular filtering device. This AMM's ability to tailor phase pattern was also shown in the paper. Fleury *et al*. [35] also applied the near-zero-density concept to realize extraordinary sound transmission through ultranarrow channels in which membranes were periodically arranged. Numerical simulations were performed. The viscosity effect in the small channel, however, was not considered, which could have a significant adverse impact on the transmission. Park *et al*. [81] constructed walls perforated with sub-wavelength holes and membranes were installed across the holes to introduce zero-mass at certain frequencies. At these frequencies, extraordinary sound transmission can be observed, essentially making a wall "invisible" to sound and could have potential applications in sound filtering and audio microscope. Gu *et al*. [82] designed a 2D network of membrane-type AMMs to demonstrate cloaking, high transmission through sharp corners, and wave splitting at the density-near-zero frequency. Other papers on the topic of membrane- or plate-type AMMs without masses can be found in [34], [51], [83]–[88].

2.2.4 Active AMMs

Active AMMs is a concept to give passive AMMs the capability to actively tune the resonance frequency as well as other parameters and was initially introduced and studied by Baz in 2009 [89] and 2010 [90]. Specifically, the membranes used in the active AMMs were piezoelectric diaphragms and could yield constant effective density over a wide frequency band. The effective density control was achieved by the active capacitance resulted from self-sensing feedback, tuning capacitance and inductance controlled by the applied voltage. Later on, Akl and Baz extended the analysis of tunable effective density from one unit cell to multi-cells [91]. The same authors also created an active AMM with programmable bulk modulus by attaching a piezoelectric diaphragm on the bottom of a resonator cavity (Helmholtz resonator) [92]. Their proposed AMMs were experimentally demonstrated [93][94], which showed that the effective density of the AMM unit cell could be tuned to a value greater or less than the density of water.

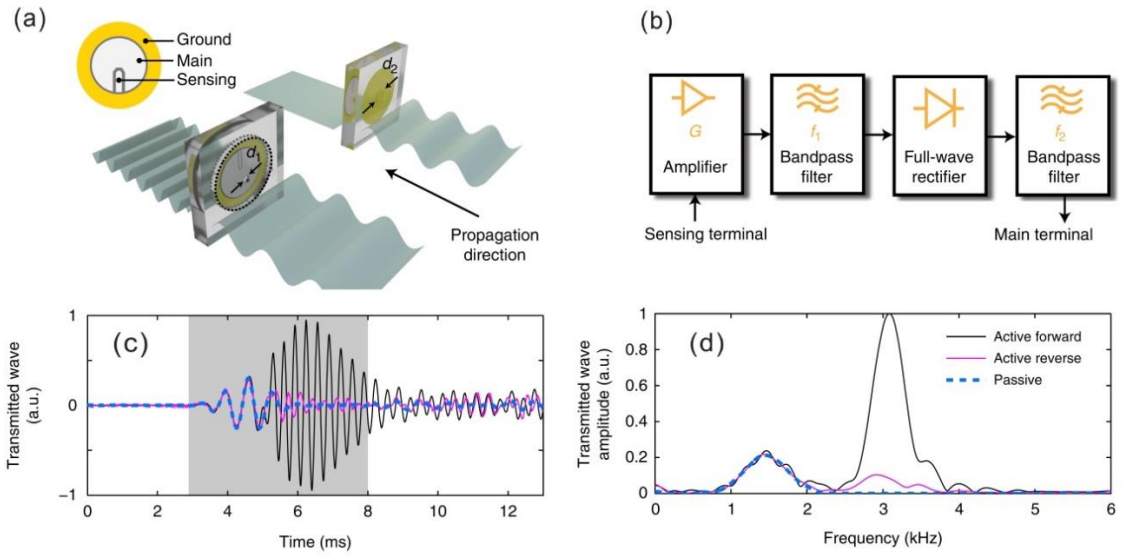

Figure 2.8. (Color online) The non-reciprocal active AMM. (a) The unit cell allows acoustic waves to pass in one direction and blocks acoustic waves in the opposite direction. (b) The electronic circuit to drive the membrane using the piezoelectric patch. The transmitted wave vs. (c) time and (d) frequency in three cases: cell powered in the forward direction, cell powered in the reverse direction, and unpowered cell. When the cell is powered and the sound is in the forward direction, the transmission is high at the operating frequency, otherwise the transmission is low, leading to the desired non-reciprocity. Taken from Popa *et al.* [6].

Following the similar working principle in [93][94], Popa *et al.* [95] fabricated two compact unit cells consisted of a sensing transducer and one or two PZT diaphragms. These unit cells were installed in a waveguide to test the performance. In the case of a unit cell with only one PZT diaphragm, the PZT diaphragm was actuated to behave as a dipole source so that the effective mass of the unit cell could be controlled. On the other hand, in the case of a unit cell with two adjacent PZT diaphragms, the two PZT diaphragms were actuated to behave as a monopole source which led to tunable effective bulk modulus. Popa *et al.* [6] also designed, fabricated, and tested a highly nonlinear and non-reciprocal active AMMs based on piezoelectric membranes (Fig. 2.8). The sample

consisted of the sensing part, actuating part and two subwavelength Helmholtz cavities tuned on different frequencies. A piezoelectric membrane was utilized for sensing and actuating, but essentially behaved as a second harmonic generator (double the incoming wave frequency). The two Helmholtz cavities were responsible for controlling the asymmetrical transmission. An isolation factor of > 10dB was observed around 3 kHz. Most recently, the same group built an AMM slab utilizing piezoelectric membranes [96]. They showed that such an AMM can be used as an acoustic lens whose properties are reconfigurable in real time. Imaging at the 2^{nd} harmonics was demonstrated to beat the diffraction limit of the fundamental frequency.

Zhang *et al.* [97] proposed an active plate-type AMM which is composed of a thin plate with shunted piezoelectric patches attached on both sides. STL was calculated by the effective medium method. Compared with the un-shunted case, shunted piezoelectric patches could lead to higher STL. The high STL region can also be broadened by negative capacitance shunting circuits. Other similar papers on active AMMs using piezoelectric elements can be found in [98]–[100].

Instead of using piezoelectric elements, Chen *et al.* [101] proposed a non-contact method to actively tune the effective density of their membrane-type AMMs. Particles of magnetorheological elastomers were embedded in elastic membranes. Under the external gradient magnetic field, the prestress and rigidity of the membrane can be changed so that the resonance frequency can be tuned. Xiao *et al.* [102] proposed a modified membrane-type AMM, which is composed of a metal-coated central platelet on a membrane and a rigid mesh electrode placed above the platelet, to achieve active tuning. With increased DC voltage applied on the mesh electrode and metal-coated platelet, the first

eigenfrequency of the membrane and the phase of the transmitted wave can be adjusted. The tunable frequency range was up to 70 Hz. Attaching one passive platelet and one active platelet on a membrane can generate an acoustic switch at the resonance frequency of the active platelet. With phase-matched AC voltage applied on the electrodes, the AMM can be an amplifier or a muffler.

Using electroacoustic resonators is another potential method to achieve active AMMs that can potentially inspire the development of membrane or plate-type AMMs. Lissek [103] proposed that an electroacoustic resonator (a loudspeaker) shunted with a series RLC circuit can achieve a feedback-based active impedance control. It has the capability to match acoustic impedance for total absorption or to produce negative acoustic impedance for sound reflection. Fleury *et al.* [104] proposed a parity-time symmetry acoustic sensor by utilizing two loudspeakers. The first loudspeaker connected with a passive electrical circuit absorbs impinging acoustic wave whereas the second loudspeaker connected with an active electrical circuit can produce the time-reversed signal of the first loudspeaker to compensate for the reflected and scattered acoustic field from the first loudspeaker. This acoustic sensor therefore could measure the sound field without affecting it.

2.3 Summary

Although there has been a substantial development for membrane- and plate-type AMMs, some limitations and challenges should be addressed. The rapid development of these AMMs is largely driven by their potential applications. Out of the many applications proposed by researchers, noise reduction seems to be a particularly

promising one. A number of applications, including cloaking [33], cancelling out aberrating layers [5], super-absorption [60], and subwavelength imaging [31][32], can be challenging to achieve and control in practice due to the requirement of high precision fabrication of the microstructures in order to achieve the accurate effective medium properties of the AMMs. In addition, passive membrane- and plate-type AMMs are liable to strong dispersion, i.e., the effective medium properties are highly frequency dependent. Consequently, most devices targeting these applications operate in a rather narrow frequency band. On the other hand, the noise reduction performance of membrane- and plate-type AMMs do not rely on precise effective medium properties, i.e., as long as the effective density is negative, large sound transmission loss can be expected. More importantly, due to the lightweight nature of the membrane and thin plate, lightweight noise reduction panels can be designed and constructed to battle low-frequency noise which has been a longstanding issue in both academia and industry. For example, Sui *et al*. [30] experimentally demonstrated that a lightweight thin-plate AMM having a mass per unit area at 1.3 kg/m^2 could yield STL consistently higher than 45 dB below 500 Hz. This type of AMMs could be extremely useful in aerospace and automotive industries where weight is considered critical. Previous studies, however, have not validated this type of noise reduction panel on a large scale conforming to standard American Society for Testing and Materials (ASTM) STL testing. The true potential of the AMM based noise reduction panel therefore has yet to be evaluated.

For a majority of membrane-type AMMs, the performance is sensitive to the tension applied to the membrane. Unfortunately, tension is difficult to control and maintain over a long period of time (e.g., tension could change dramatically as time progresses or with a

slight variation in temperature or humidity). The requirement of accurate and uniform tension also adds extra complexity to the fabrication process. In this aspect, the plate-type AMMs seem to have an advantage since tension is not required. However, plate-type AMMs could be liable to a greater amount of energy loss, which is undesirable in most applications. This is particularly a problem near the resonance frequency, for example, when the plate-type AMMs are used to achieve near-zero effective density [34]. Consequently, the choice of the plate material is critically important as some materials could be very lossy, such as polymers. In addition, as plate-type AMMs' performance depends on the plate material properties, they could be highly frequency dependent or could vary under temperature change. These facts should be more carefully considered and taken into account by future study on plate-type AMMs.

Three-dimensional (3-D) manufacturing of membrane- and plate-type AMMs is also challenging. A number of advanced manufacturing techniques have been utilized for fabricating AMMs, including computer numerical control (CNC) machining [105], laser cutting [37], and 3-D printing [40]. However, most membrane- and plate-type AMMs have been fabricated manually, limiting the prototypes to operate at relatively low frequencies. This is partially because the fabrication of membrane- and plate-type AMMs could require multiple different materials simultaneously. This can be potentially circumvented by 3-D printing, as some sophisticated 3-D printing machines have the capability of printing using multiple different materials. Nevertheless, the precision and resolution of most commercial 3-D printers still do not meet the requirement of high frequency AMMs (> 100 kHz). Even for kHz range sound, the thickness of membranes or plates could be in the 100 micron range, challenging the most advanced 3D printers on

the market today. More advanced manufacturing technologies therefore need to be developed for high resolution fabrication and mass production of membrane- and plate-type AMMs.

Chapter III

On the Evaluation of Effective Density for Plate- and Membrane-type AMMs without Mass attached

To use plate- or membrane-type AMMs for designing devices controlling acoustic waves, it is critically important to know exactly the effective density for a given AMM structure. For example, in designing complimentary metamaterials (CMMs) [5], the effective density needs to be tuned to a certain value in order to perfectly cancel out the unwanted aberrating layer. Although the effective density of an AMM based on circular plates can be calculated using a lumped model [1], no explicit derivation of effective density has been reported for square membranes and plates, which were used in recent studies [5][29]. This chapter aims to theoretically and numerically investigate the membrane- and plate-type AMMs without mass attached. The acoustic impedances of square plates and membranes under uniform acoustic pressure are first computed. This is accomplished by three different approaches: analytic models, approximate models, and FEM. The effective density can be then estimated for plate- and membrane-type AMMs using the lumped model.

3.1 Plate-type AMMs without mass attached

3.1.1 Analytic model for the acoustic impedance of a square, clamped plate

Although this section focuses on square plates as they have been used recently for building two dimensional (2D) negative density CMMs [5], the analytic model presented here is generic and can be readily used for rectangular plates. The analytic approach presented here is similar to that in [106], in which the plate vibration under point forces, couples and piezomoments were studied. For a thin, clamped plate under a net sound pressure $P(x,y,t)$, the governing equation of the transverse displacement $W(x,y,t)$ is the flexural wave equation which reads

$$D\nabla^4 W(x,y,t) + \rho h \frac{\partial^2 W(x,y,t)}{\partial t^2} = P(x,y,t), \tag{3.1}$$

where D is the flexural rigidity and $D = Eh^3 / 12(1-v^2)$; E, v, ρ and h are the Young's Modulus, Poisson's ratio, density and thickness of the plate, respectively.

Assuming harmonic excitations with angular frequency ω, $P(x,y,t)$ and $W(x,y,t)$ can be written as

$$P(x,y,t) = p(x,y)e^{j\omega t},\ W(x,y,t) = w(x,y)e^{j\omega t}. \tag{3.2}$$

$p(x,y)$ and $w(x,y)$ can be expanded by eigenfunctions as

$$p(x,y)=\sum_{m=1}^{\infty}\sum_{n=1}^{\infty}p_{mn}\varphi_{mn}(x,y)\ ,\ w(x,y)=\sum_{m=1}^{\infty}\sum_{n=1}^{\infty}w_{mn}\varphi_{mn}(x,y)\,, \tag{3.3}$$

where $\varphi_{mn}(x,y)$ can be further decomposed using the separation of variables, i.e., $\varphi_{mn}(x,y)=X_m(x)Y_n(y)$. $X_m(x)$ and $Y_n(y)$ are chosen to be the same as the eigenfunctions for a beam clamped on both ends to satisfy the clamped boundary condition (the transverse displacement and slope of plate are zero) and the equation of motion for the plate. They are given by

$$X_m(x)=J\left(\frac{\lambda_m x}{a}\right)-\left[\frac{J(\lambda_m)}{H(\lambda_m)}\right]H\left(\frac{\lambda_m x}{a}\right),\ Y_n(y)=J\left(\frac{\lambda_n y}{a}\right)-\left[\frac{J(\lambda_n)}{H(\lambda_n)}\right]H\left(\frac{\lambda_n y}{a}\right), \tag{3.4}$$

where a is the width of the square plate, $J(u)=\cosh(u)-\cos(u)$, $H(u)=\sinh(u)-\sin(u)$. λ_m or λ_n satisfies the equation $\cosh(\lambda)\cos(\lambda)=1$.

Combing Eqs. (3.2)-(3.4), $P(x,y,t)$ and $W(x,y,t)$ can be obtained and substituted into Eq. (3.1), w_{mn} can be then written as

$$w_{mn}=\frac{\int_0^a\int_0^a p(x,y)X_mY_n dxdy}{D(I_1I_2+2I_3I_4+I_5I_6)-\rho h\omega^2 I_2I_6}, \tag{3.5}$$

where

$I_1=\int_0^a X_m^{(4)}X_m dx$, $I_2=\int_0^a Y_n^2 dy$, $I_3=\int_0^a X_m{}''X_m dy$, $I_4=\int_0^a Y_n{}''Y_n dy$, $I_5=\int_0^a Y_n^{(4)}Y_n dy$, $I_6=\int_0^a X_m{}^2 dx$ and the superscript in "()" indicates the order of the derivative and double prime is the 2nd order derivative.

At the resonance frequencies, w_{mn} reaches infinity in the absence of damping. The resonance angular frequencies can thus be obtained by setting the denominator of Eq. (3.5) to zero, which leads to

$$\omega_{mn} = \sqrt{\frac{D\left(I_1 I_2 + 2I_3 I_4 + I_5 I_6\right)}{\rho h I_2 I_6}}\,. \tag{3.6}$$

The acoustic impedance of a vibrating plate is defined as

$$Z_{am} = \frac{\int_0^a \int_0^a P\left(x, y, \mathrm{t}\right) dxdy}{\bar{V}\left(t\right) a^4} = \frac{\int_0^a \int_0^a P\left(x, y, t\right) dxdy}{\dfrac{\partial \bar{W}\left(t\right)}{\partial t} a^4} = \frac{\int_0^a \int_0^a p\left(x, y\right) dxdy}{j\omega \bar{w} a^4}\,, \tag{3.7}$$

where $\bar{V}$, $\bar{W}$ and $\bar{w}$ are the average velocity, transverse displacement, and magnitude of transverse displacement, respectively.

Consider a subwavelength size waveguide (Fig. 3.1(a)), plane waves with normal incidence angle can be assumed. $p\left(x, y\right)$ is therefore a constant p_0 (uniform distribution) and Eq. (3.7) becomes

$$Z_{am} = \frac{1}{j\omega \int_0^a \int_0^a \left[\sum_{m=1}^{\infty} \sum_{n=1}^{\infty} \dfrac{\int_0^a \int_0^a X_m Y_n dxdy}{D\left(I_1 I_2 + 2I_3 I_4 + I_5 I_6\right) - \rho h \omega^2 I_2 I_6} X_m Y_n \right] dxdy}\,. \tag{3.8}$$

Equation (3.8) is computed numerically using Matlab. Specifically, the Simpson's 3/8 rule is applied to approximate the integrals.

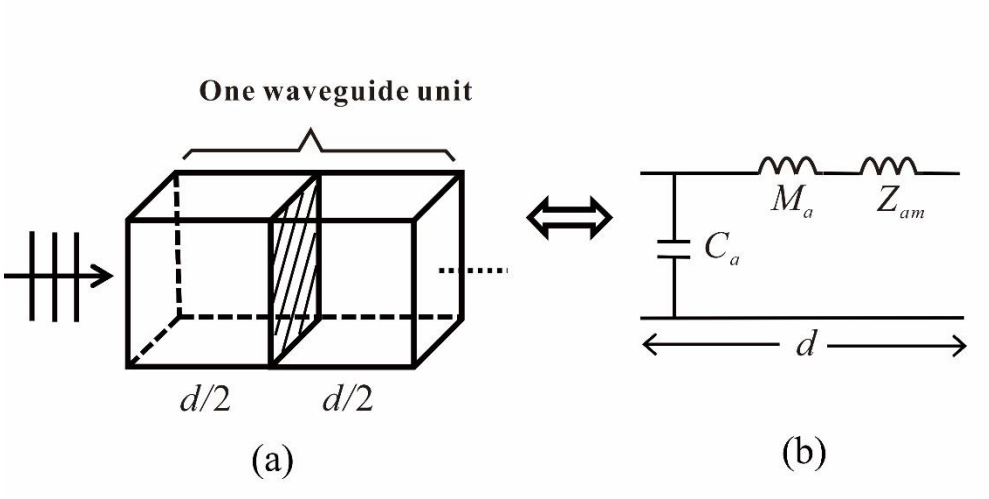

Figure 3.1. (a) Schematic of a single unit cell with a length *d* for plate- or membrane type AMMs without mass attached. (b) The lumped model for plate- or membrane type AMMs. Z_{am} represents the acoustic impedance of the plate or membrane.

3.1.2 Approximate model for the acoustic impedance of a square, clamped plate

The acoustic impedance Z_{am} of a plate can be divided into two parts at low frequencies (frequency around or below the first resonance frequency of the plate). They are the acoustic compliance (C_{am}) and acoustic mass (M_{am}) in the lumped model [1] (Fig. 3.1(b)). In other words,

$$Z_{am} = \frac{1}{j\omega C_{am}} + j\omega M_{am}. \tag{3.9}$$

When the frequency of interest is significantly below the first resonance frequency of the plate, the acoustic compliance term will dominate and the acoustic mass term can be

ignored. Therefore, C_{am} can be determined by computing Z_{am} at an extremely low frequency using Eq. (3.9). Similar to circular plates, it is assumed that the acoustic compliance is associated with the dimensions and flexural rigidity [1]. By equating the unit of Z_{am} ($kg/m^4 s$) and the unit of the term containing C_{am} ($1/j\omega C_{am}$) in Eq. (3.9), the unit of C_{am} is calculated to be $m^4 s^2/kg$. Consequently, the power for D ($kg \cdot m^2/s^2$) must be -1 and the power for a (m) must be 6. The formula for C_{am} is found to be

$$C_{am} = 3.73 \times 10^{-4} \frac{a^6}{D} . \tag{3.10}$$

Note that Z_{am} should be zero at the first resonant frequency (ω_{11}) of the plate. Hence, M_{am} can be analytically obtained from Eq. (3.9) as

$$M_{am} = \frac{1}{\omega_{11}{}^2 C_{am}} , \tag{3.11}$$

where $\omega_{11} = \frac{C_0}{a^2}\sqrt{\frac{D}{\rho h}}$ and C_0 is a constant [107]. Substituting Eq. (3.10) into Eq. (3.11) yields

$$M_{am} = \frac{1}{3.73 \times 10^{-4} C_0{}^2} \frac{\rho h}{a^2} = C_1 \frac{\rho h}{a^2} . \tag{3.12}$$

To determine the constant C_1, ω_{11} is first computed using the analytic model (Eq. 3.6) for a random plate, M_{am} can then be calculated using Eq. (3.11) since both C_{am} and ω_{11}

are known. Finally, C_1 is determined from Eq. (3.12). Since C_1 is independent of the dimensions and properties of the plate, the obtained C_1 is general and it is found that

$$M_{am} = 2.06\frac{\rho h}{a^2}. \tag{3.13}$$

Equations (3.10) and (3.13) provide the acoustic compliance and acoustic mass for the approximate model to predict the acoustic impedance for a square, clamped, thin plate. It is noted that the acoustic compliance is proportional to a^6 for square plates whereas it is proportional to r^6 (r being the radius) for circular plates [1].

3.1.3 FEM model for the acoustic impedance of a square, clamped plate

To verify the analytic and approximate models, a commercial FEM package COMSOL is adopted to analyze the vibration of a clamped plate under a certain surface pressure. The solid-acoustic interaction module is used. As indicated by Eq. (3.7), the acoustic impedance of the plate, Z_{am}, can be extrapolated using the average surface velocity and the net pressure on the plate obtained from the FEM simulation. Two distinct FEM models are used to achieve this goal. In the first model, a boundary load is directly applied on the top surface of the clamped plate. The net pressure is therefore F/a^2, where the F is force in Newton. In the second model, a waveguide is created where clamped plates are placed inside in a periodical manner (Fig. 3.1(a)). A plane wave enters from one side and the end of the waveguide is set up to be a non-reflecting boundary. The acoustic pressures on two planes extremely close to the plate are obtained in order to

compute the net pressure. These two models are denoted the FEM-boundary model and FEM-waveguide model, respectively. For both FEM models, convergence studies are carried out in order to ensure most accurate results.

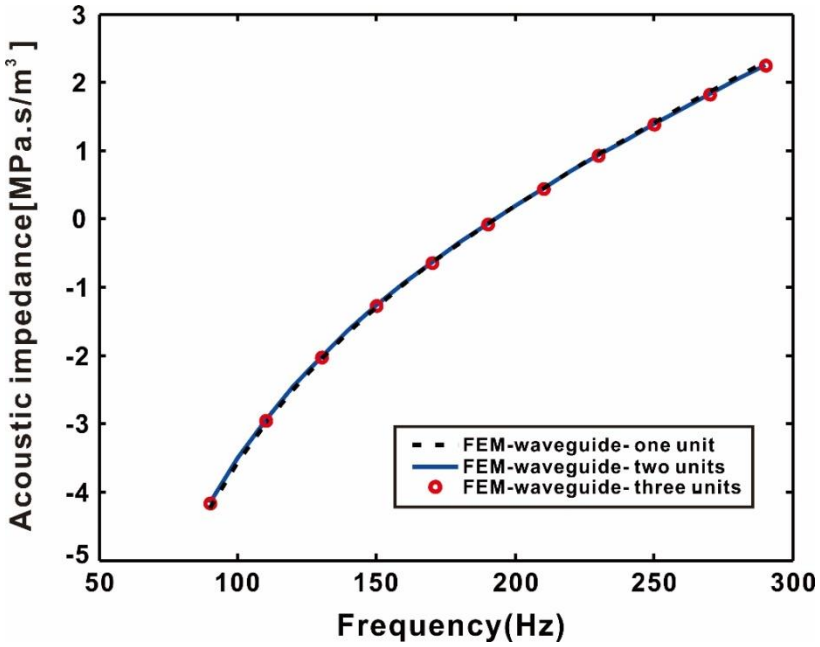

Figure 3.2. (color online) The acoustic impedances predicted by the FEM waveguide model with one, two and three unit cells, respectively.

Consider a rubber plate ($E = 10MPa$, $v = 0.49$ and $\rho = 1000 kg/m^3$) with dimensions $a = 10mm$ and $h = 0.1mm$ as a study case. The first resonance frequency of this plate is at around 190 Hz. The length of the unit cell is $2mm$. The acoustic impedance can be calculated using the three different methods presented above. Since in the FEM-waveguide model, the plate number can be varied. We first examine whether

the number of plates (units) would change the calculated acoustic impedance. Figure 3.2 illustrates the acoustic impedance obtained from the FEM-waveguide model with various numbers of units. Only the imaginary part of the acoustic impedance is shown since the real part is zero. Due to the large computation, the maximum unit number considered here is three. In all three simulations, the acoustic impedance is extracted for the first plate in the waveguide. However, additional simulations show that the acoustic impedances extracted from other plates (2^{nd} and the 3^{rd} plate) are almost identical.

Figure 3.2 indicates that having multiple waveguide units will not significantly affect the acoustic impedance of a plate. This result is expected because the same plate with the same boundary condition should have identical acoustic impedance as long as the excitation conditions (uniform pressure on the plate) are also the same.

Figure 3.3 shows the comparison among different models for the acoustic impedance. One can observe slight discrepancy between the analytic and simulation (FEM) results, which is possibly caused by the approximations in the flexural wave equation for a thin plate and inevitable numerical errors in FEM. Because the lumped model is accurate only around and below the resonance frequency [1], the approximate model becomes less accurate when the frequency is significantly higher than the resonance frequency (190 *Hz*). At low frequencies, the approximate model agrees very well with the analytic model. Around the resonance frequency, the acoustic impedance is near zero, as expected. The phase difference between the net pressure on the plate and vibrating velocity changes by 180° as the frequency transitions from below ω_{11} to above ω_{11}, so that the impedance transitions from being negative to positive.

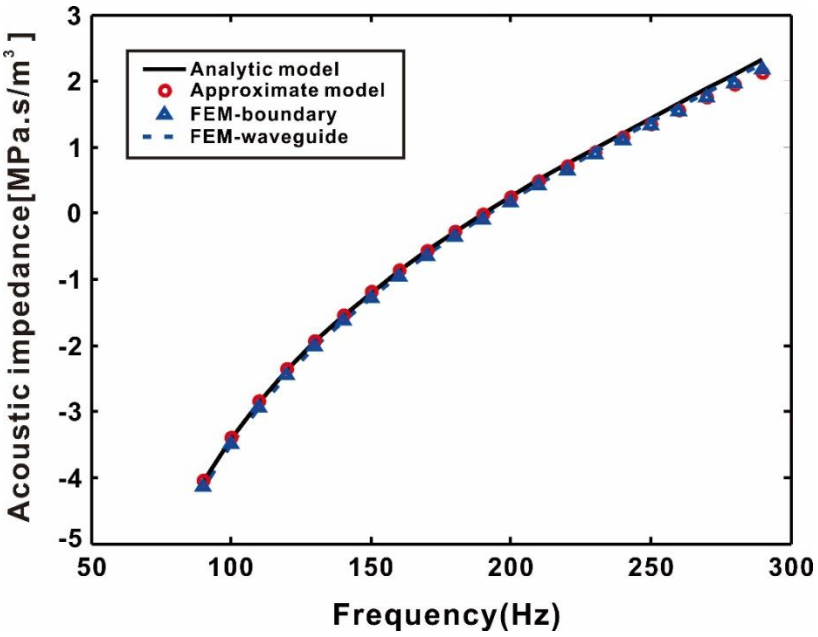

Figure 3.3. (color online) The acoustic impedances predicted by the analytic model, approximate model, FEM-boundary model and FEM-waveguide model.

3.1.4 Effective density

Since the wavelength of the incident sound wave is much larger than the unit size, the AMM (Fig. 3.1(a)) can be regarded as an effective homogeneous media whose effective density ρ_{eff} can be evaluated. Under the low frequency approximation, the lumped model [1] (Fig. 3.1(b)) can be employed to predict the effective density of the AMMs. The acoustic medium can be approximated by a shunt acoustic compliance (C_a) and a series acoustic mass (M_a) which are given by

$$M_a = \frac{\rho_0}{a^2} d \,,\; C_a = \frac{a^2}{K} d \,, \tag{3.14}$$

where ρ_0 is the density of the acoustic medium and is chosen as air ($1.2 kg/m^3$) in this study; K is the bulk modulus of the acoustic medium and d is the length of a unit cell assuming the thickness of the plate/membrane is negligible. Otherwise the length of the unit cell is $d+h$. When the rubber plate vibrates, the surrounding acoustic medium will behave like added mass to resist the vibration so that Z_{am} is in series with M_a.

The effective density (ρ_{eff}) of this waveguide unit can be obtained as [1]

$$\rho_{eff} = \frac{\left(j\omega M_a + Z_{am} \right) a^2}{j\omega d}. \tag{3.15}$$

Substituting Eqs. (3.9), (3.10) , (3.13) and (3.14) into Eq. (3.15), an approximate model for predicting the effective density can be established and the equation reads

$$\rho_{eff} = \rho_0 - \frac{2.68\times 10^3 D}{\omega^2 a^4 d} + \frac{2.06\rho h}{d}. \tag{3.16}$$

To verify the accuracy of the lumped model, a finite-difference approximation method [5][27][108] is used to retrieve the effective density for the structure shown in Fig. 3.1(a). In this approach, the FEM is first used to compute the sound field in the waveguide and the calculated pressure and velocity are used to estimate the effective density. This approach is denoted the FEM-finite difference approach. Starting from the 1-D Euler's equation, the pressure *p* and the velocity *v* are related by

$$\frac{dp}{dx} = -j\omega\rho_{eff} v. \tag{3.17}$$

Assuming the unit cell size is considerably smaller than one wavelength, Eq. (3.17) can be rewritten using the finite-difference approximation as

$$\frac{\Delta p}{d} = -j\omega\rho_{eff}\bar{V}, \tag{3.18}$$

where $\Delta p = p_1 - p_2$; p_1 and p_2 are the pressures at the right end and left end of the unit cell, respectively; $\bar{V}$ is the average transverse velocity on the plate. By using Δp and $\bar{V}$ obtained from FEM simulations, the effective density can be calculated as

$$\rho_{eff} = \frac{\Delta p}{d}\frac{j}{\omega\bar{V}}. \tag{3.19}$$

Figure 3.4(a) shows the effective density predicted by the analytic model, approximate model, and the FEM-finite difference model. Only the real part of the density is shown as the imaginary part is negligible (exactly equal to zero in the analytic and approximate models). For the FEM-finite difference model, the number of unit cells varies from one to three. Similar to the acoustic impedance case, no significant change is observed. The analytic and approximate models agree well with the FEM-finite difference model. The slight discrepancy is expected as they do not produce exactly the same acoustic impedance as that predicted by the FEM models (Fig. 3.3). When the frequency is below the first resonance frequency of the square clamped plate (around 190 *Hz*), the effective density is negative. This is because the velocity is 90° out of phase with the acceleration (*a*) and therefore the acceleration is 180° out of phase with the pressure/force (*F*). By forcing the Newton's second law *F* = *ma*, *m* must be negative. When the frequency is above the first resonance frequency, the unit vibrates reversely

(180° phase change) and the net pressure on the unit is in phase with the vibrational acceleration of the plate and the effective density becomes positive. It is worthwhile to mention that, a simple equation has been proposed to predict the effective density of plate- or membrane-type AMMs without mass attached, which reads [27]

$$\rho_{eff}' = \rho(1-\frac{\omega_c^2}{\omega^2}). \tag{3.20}$$

This equation, however, predicts the effective density of the vibrating plate or membrane alone without considering the fluid in the waveguide, whereas we took both the plate and the fluid in the waveguide into account and treated them as a homogenized medium to evaluate the effective density. The effective density predicted by Eq. (3.20) can be seen in Fig. 3.4(b), which is dramatically different from those in Fig. 3.4(a), although they both show near-zero density around the resonance frequency.

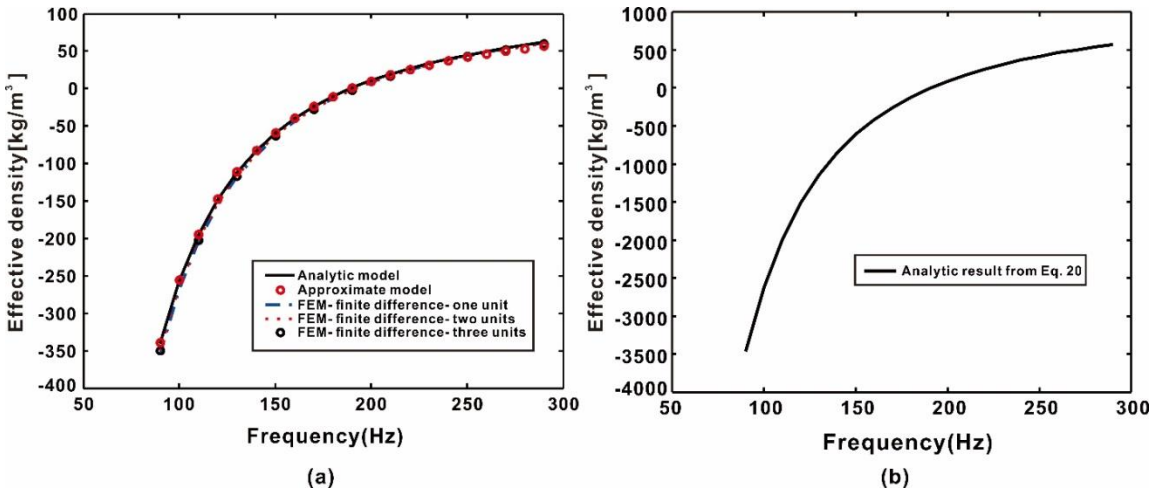

Figure 3.4. (color online) The effective density of the plate-type AMM. (a) Results produced from three different models. (b) Results predicted from Eq. (3.20).

The next case considers the effect of damping of the plate. The damping is taken into account *ad hoc* by considering a loss factor α so that the Young's modulus of the plate becomes a complex number, i.e., $E' = E(1+ j\alpha)$. This E' is used to calculate the flexural rigidity *D*, which further leads to the acoustic impedance and the effective density using Eqs. (3.15) and (3.16). Two values of frequency independent loss factor are considered, i.e., 0.1 and 0.3. The real part of effective density, shown in Fig. 3.5(a), remains the same as the case without considering the damping. As the loss factor increases, the magnitude of the imaginary part of effective density also increases as shown in Fig. 3.5(b). In addition, the imaginary part of the effective density is always negative which introduces further energy loss to the sound transmission. It is noted that the sign of the imaginary part of the density depends on whether $e^{j\omega t}$ or $e^{-j\omega t}$ is used. In the cases studied, the imaginary part of the density is on the same order to the real part of the density, therefore the damping effect cannot be ignored for α on the order of 0.1, which is common for polymeric materials.

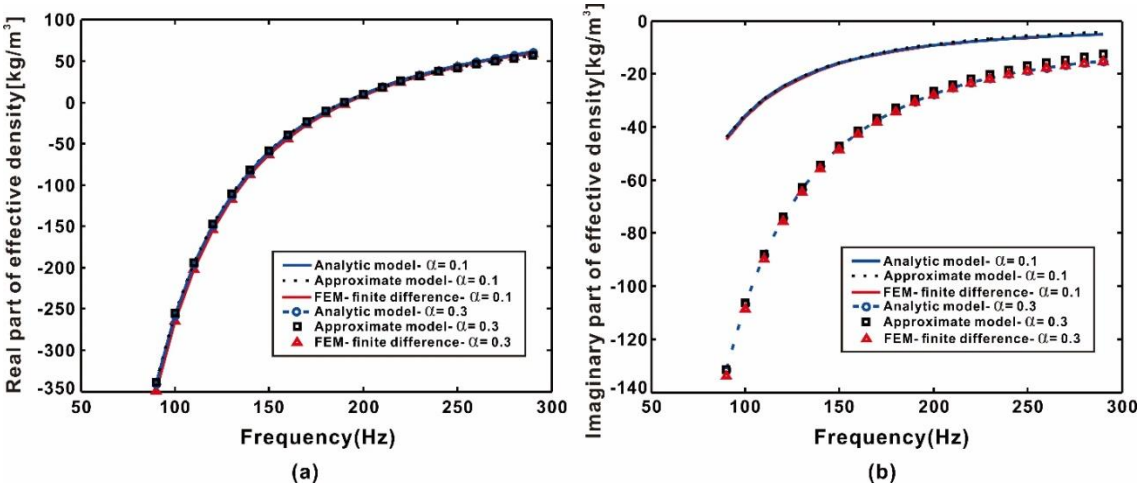

Figure 3.5. (color online) The effect of the loss factor α on the effective density. α is chosen as 0.1 and 0.3. (a) Real part of the effective density. (b) Imaginary part of the effective density.

To further validate the predicted effective density, transmission coefficients through plate-type AMMs are also computed and compared among different models. The pressure reflection and transmission coefficients through a homogeneous medium are given by [71]

$$R = \frac{Z_m{}^2 - Z_0{}^2}{Z_0{}^2 + Z_m{}^2 + 2jZ_0Z_m\cot(\phi)},\ T = \frac{1+R}{\cos(\phi) - \dfrac{Z_m j\sin(\phi)}{Z_0}}, \tag{3.21}$$

where $Z_m\,(=\rho_{eff}c_{eff})$ is the characteristic impedance of the waveguide. $c_{eff} = \sqrt{B_{eff}/\rho_{eff}}$ where B_{eff} is the effective bulk modulus and c_{eff} is the effective speed of sound. It was shown that membranes/plates in the waveguide do not alter the effective bulk modulus of the medium so that B_{eff} is the same as the bulk modulus of air [109]. However, it should be kept in mind that, this is not strictly true for all cases. For instance, if the waveguide is largely composed of membranes/plates in volume, or if the background medium is

something other than air, the modulus of membranes/plates may have a non-trivial effect on B_{eff} . $Z_0 = \rho_0 c_0$ is the characteristic impedance of the air. $\phi = -2\pi fnd/c_{eff}$ is the phase change of the sound through the medium where *n* is the number of unit cells and *nd* is the total length of the AMM. If the plate thickness *h* is not negligible, *d* has to be replaced by *d*+*h*.

Using the ρ_{eff} predicted from the analytic and approximate models, the transmission coefficients of the plate-type AMMs can be calculated. To verify the results, the transmission coefficients are directly computed using FEM. Fig. 3.6 shows the transmission coefficient of a three unit plate-type AMM. Figure 3.6(a) shows the results without considering the damping whereas Fig. 3.6(b) shows the results with damping. Three different models agree very well over the frequency range under consideration. This also indicates that the presence of the plates indeed does not change the bulk modulus as assumed earlier. When there is no damping, the transmission coefficients reach the peak (1.0) at the resonance frequency as expected. With the presence of the damping, the transmission coefficients are reduced due to the energy loss in the plate. In both cases, the approximate model becomes less accurate at a frequency significantly higher than the resonance frequency.

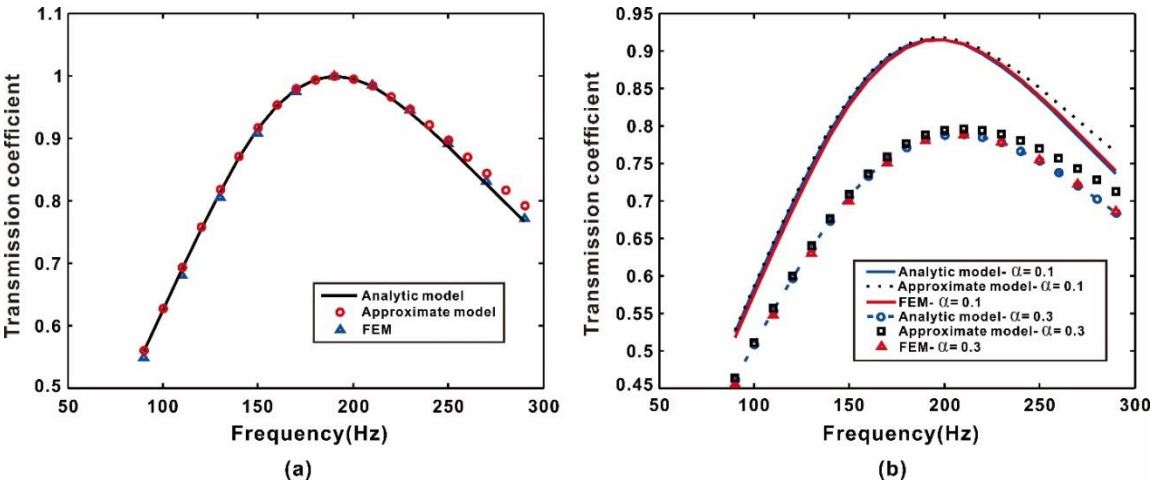

Figure 3.6. (color online) The transmission coefficient of the plate-type AMM with three unit cells. (a) Without considering the loss. (b) With loss factor α: 0.1 and 0.3.

3.2 Effective density of membrane-type AMMs without mass attached

This section focuses on the membrane-type AMMs. Similarly, the analytic model, approximate model, and the FEM model are developed to predict the acoustic impedance as well as the effective density.

3.2.1 Analytic model for the acoustic impedance of a square, clamped membrane

The governing equation of the transverse displacement $W_1(x,y,t)$ of a pre-stretched membrane under the net pressure $P_1(x,y,t)$ is [110]

$$T_1\nabla^2 W_1(x,y,t)-\rho_1 h_1\frac{\partial^2 W_1(x,y,t)}{\partial t^2}=-P_1(x,y,t), \tag{3.22}$$

where T_1 is the uniform tension per unit length; ρ_1 and h_1 are the density and thickness of the membrane, respectively.

Assuming time-harmonic solutions, i.e., $P_1(x,y,t)=p_1(x,y)e^{j\omega t}$, $W_1(x,y,t)=w_1(x,y)e^{j\omega t}$, Eq. (3.22) leads to

$$\nabla^2 w_1(x,y)+\beta^2 w_1(x,y)=-\frac{p_1(x,y)}{T_1}, \tag{3.23}$$

where $\beta=\omega\sqrt{\rho_1/T_1}$ is the wavenumber of the transverse wave on the membrane.

The eigenfunction of a clamped square membrane is well-known as [110]

$$\varphi_{1mn}(x,y) = A_1 A_3 \sin\left(\frac{m\pi x}{a}\right)\sin\left(\frac{n\pi y}{a}\right). \tag{3.24}$$

After normalization, $A_1 A_3 = 2/\sqrt{\rho_1 a^2}$.

The resonance angular frequencies can be readily derived as [110]

$$\omega_{mn} = \frac{\pi}{a}\sqrt{\frac{T_1}{\rho_1}\left(m^2+n^2\right)}. \tag{3.25}$$

$w_1(x,y)$ and $p_1(x,y)$ can be expanded using $\varphi_{1mn}(x,y)$ as

$$p_1(x,y) = \sum_{m=1}^{\infty}\sum_{n=1}^{\infty} Q_{mn}\varphi_{1mn}(x,y),\ w_1(x,y) = \sum_{m=1}^{\infty}\sum_{n=1}^{\infty} w_{1mn}\varphi_{1mn}(x,y). \tag{3.26}$$

Substituting Eq. (3.26) into Eq. (3.23), w_{1mn} can be shown as

$$w_{1mn} = \frac{1}{T_1}\frac{Q_{mn}}{\beta_{mn}{}^2 - \beta^2}, \tag{3.27}$$

where $\beta_{mn} = \omega_{mn}\sqrt{\rho_1/T_1}$ and $Q_{mn} = \int_0^a\int_0^a \rho_1 h_1 p_1(x,y)\varphi_{1mn}(x,y)\,dxdy$.

Similar to the case of plate-type AMMs in waveguides, plane waves are assumed and $p_1(x,y) = p_0$ and Q_{mn} becomes

$$Q_{mn} = \frac{2h_1 p_0\sqrt{\rho_1}}{a}\int_0^a\int_0^a \sin\left(\frac{m\pi x}{a}\right)\sin\left(\frac{n\pi y}{a}\right)dxdy = \frac{2h_1 p_0 a\sqrt{\rho_1}}{mn\pi^2}\left(1-(-1)^m\right)\left(1-(-1)^n\right). \tag{3.28}$$

Combining Eqs. (3.27) and (3.28) and then substituting the resulting equation of w_{1mn} into Eq. (3.26), $w_1(x,y)$ can be obtained as

$$w_1(x,y)=\sum_{m=1}^{\infty}\sum_{n=1}^{\infty}\frac{4p_0}{\rho_1 h_1\left(\omega_{mn}{}^2-\omega^2\right)mn\pi^2}\left(1-(-1)^m\right)\left(1-(-1)^n\right)\sin\left(\frac{m\pi x}{a}\right)\sin\left(\frac{n\pi y}{a}\right). \quad (3.29)$$

Substituting Eq. (3.29) into Eq. (3.7), the acoustic impedance of a clamped square membrane is analytically written as

$$Z_{am1}=\frac{1}{j\omega a^2\sum_{m=1}^{\infty}\sum_{n=1}^{\infty}\frac{4}{\rho_1 h_1\left(\omega_{mn}{}^2-\omega^2\right)m^2n^2\pi^4}\left(1-(-1)^m\right)^2\left(1-(-1)^n\right)^2}. \quad (3.30)$$

The summations are calculated numerically. Clearly, even number modes (m, n = 2, 4, 6…) do not contribute to the acoustic impedance, because the uniform pressure on the membrane does not excite those modes.

In contrast to plates, the acoustic impedance of the clamped membranes does not relate to the flexural rigidity (D) but rather the pre-stretched tension (T_1). The membrane model is only valid if the thickness is significantly smaller than the width and the tension is sufficiently large so that the effect of the tension dominates over that of the elasticity of the membrane.

3.2.2 Approximate model for the effective density of a square, clamped membrane

Similar to the case of plates, an approximate model for the acoustic impedance of clamped, square membranes can be derived and the acoustic compliance and mass are

$$M_{am1} = 1.44\frac{\rho_1 h_1}{a^2},\ C_{am1} = 0.035\frac{a^4}{T_1}. \tag{3.31}$$

To verify the analytic and approximate model for the acoustic impedance, the two FEM models are again used for verification. Figure 3.7 shows the results for the case where a=10mm, h_1=35μm, T_1=2MPa and d =2mm (this number d is only used in the FEM waveguide model when there are multiple membranes).

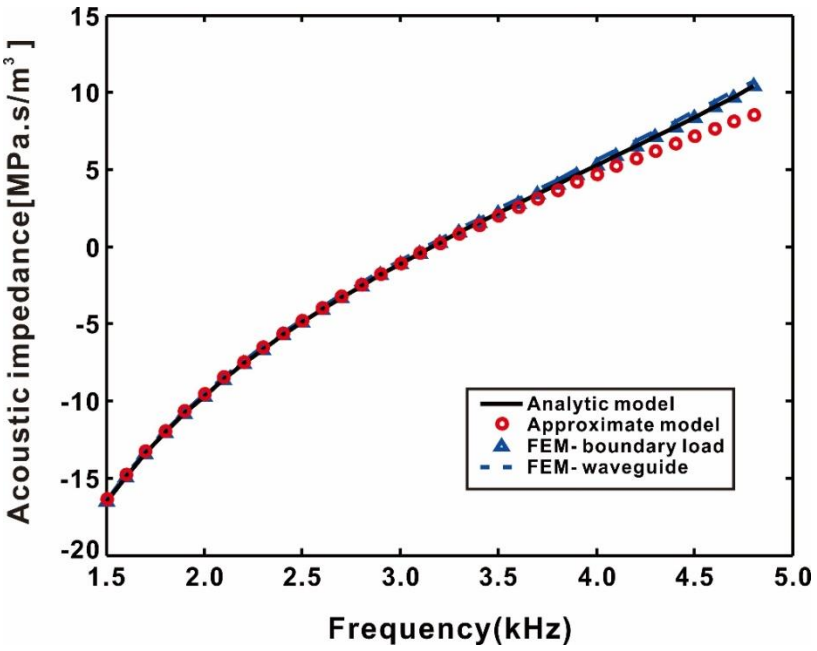

Figure 3.7. (color online) The acoustic impedance of a clamped square membrane predicted by the analytic model, approximate model, FEM-boundary model and FEM-waveguide model.

Similar to plates, only the imaginary part of the impedance is shown here. The acoustic impedance of the membrane is zero at the first resonance frequency (around $3162 Hz$ in this case) and is negative below that frequency. The analytic and the two FEM models agree well throughout the entire frequency range. The approximate model becomes less accurate at frequencies above the resonance frequency. The damping effect is not studied here for membranes because it is expected to be negligible since the thickness is extremely small. However, it is still possible to force the damping by using a complex number for the tension.

3.2.3 Effective density

After obtaining the acoustic impedance, the effective density can then be calculated by using Eq. (3.15). Substituting Eq. (3.31) into Eq. (3.15), the equation for predicting the effective density from the approximate model reads

$$\rho_{eff\,1} = \rho_0 - \frac{28.57 T_1}{\omega^2 a^2 d} + \frac{1.44 \rho_1 h_1}{d}. \tag{3.32}$$

Figure 3.8 presents the effective density predicted by the three different approaches. The FEM-finite difference approach is used to verify the analytic and approximate models. All models agree well below the resonance frequency. Similar to the plate-type acoustic metamaterial, the approximate model is less accurate above the resonance frequency. However, the approximate model could still be useful because the frequency of interest is typically below the resonance frequency where the effective density is negative.

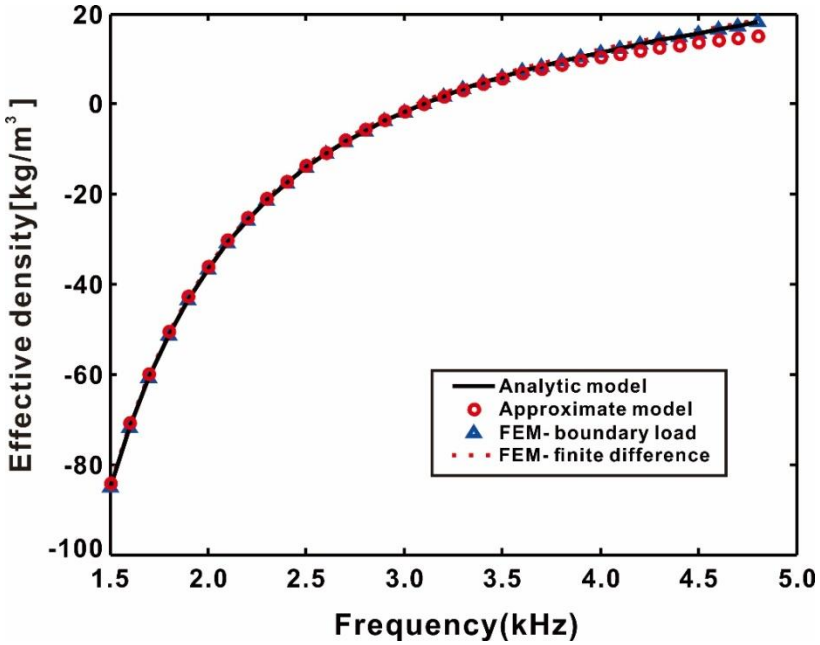

Figure 3.8. (color online) The effective density of the membrane-type AMM.

Since for square, clamped membranes, a closed form solution for the displacement can be found, the analytic model is expected to be more accurate than that of plates. Finally, Fig. 3.9 illustrates the sound transmission coefficient for the membrane-type AMM as shown in Fig. 3.1(a). Three unit cells are considered with a total length 2×3=6 mm. Results from the three models are in good agreement.

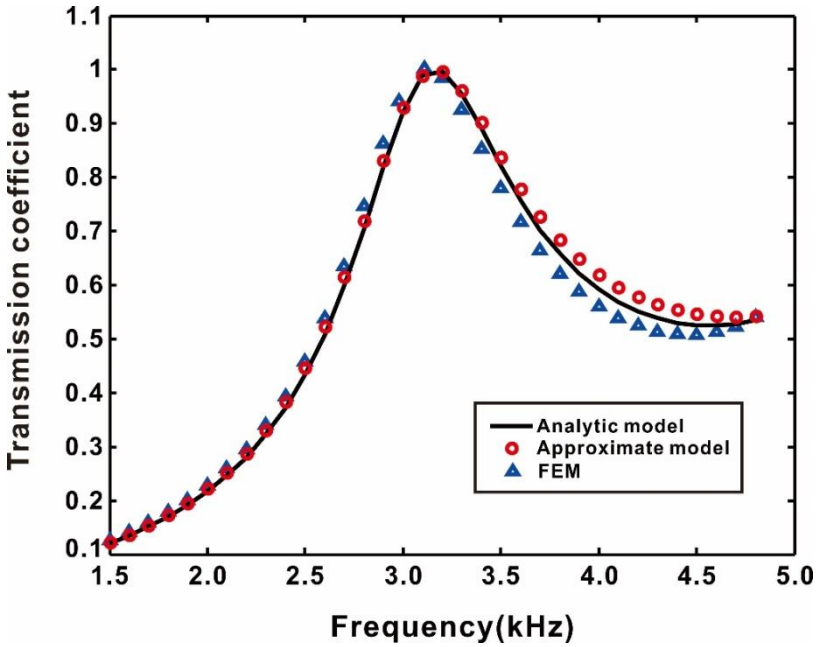

Figure 3.9. (color online) The transmission coefficient of the membrane-type AMM with three unit cells.

3.3 Summary

This chapter presents methods for predicting the effective densities of plate- and membrane-type AMMs without mass attached. The analytic model and the approximate model, which is derived from the analytic model under the low frequency approximation, are developed and their results are compared with those from the FEM model. Good agreement is found among these models when predicting the acoustic impedance, effective density, and the transmission coefficients. Although the approximate model is only accurate at frequencies below the first resonance frequency, it provides a quick and reasonably accurate approach for predicting the effective densities of plate- and membrane-type AMMs. The influence of the loss factor of the plate on the effective

density and transmission coefficient is investigated. The addition of the loss factor introduces the imaginary part of the effective density and reduces the transmission coefficient. It is assumed square plates and membranes in this work. The framework provided, however, can be applied to studying rectangular plates and membranes.

Chapter IV

Investigation of the Effective Density of Arbitrarily Shaped Plate-type AMMs without Mass attached

Based on different applications, such as honeycomb structures with hexagonal plates [30], different shapes of plates of AMMs could be required. Moreover, tuning the shapes of plates can serve as an alternative means to tune effective densities of AMMs, which could be useful when there are restrictions on adjusting the material dimensions or properties.

The aim of this chapter is to develop a procedure for evaluating effective densities of arbitrarily shaped plate-type AMMs. While FEM can be applied to this type of problem [28], it is often time-consuming and not ideal for design or optimization purposes. A meshless boundary method [111][112] without employing the concept of "finite element" was proposed to study the free vibration of arbitrarily shaped plates. In this chapter, it will be modified to study the forced vibration of arbitrarily shaped plates and will be utilized to calculate the acoustic impedances of arbitrarily shaped plates so that the effective densities of AMMs can be evaluated subsequently using the lumped model. Plates with three different shapes, i.e. circle, triangle, and hexagon, are used to demonstrate how the meshless boundary method works for the evaluation of effective densities of plate-type AMMs with arbitrary shapes.

4.1 Theory

4.1.1 Meshless boundary method

This section focuses on solving the dynamic response of a fully clamped arbitrarily shaped plate in a one-dimensional (1-D) acoustic waveguide (Fig. 4.1(a)). Consider a plate placed in a waveguide under harmonic acoustic excitations with angular frequency ω, the flexural wave equation with forced vibration can be written as [28]

$$\nabla^4 w(x,y) - \frac{\rho h \omega^2}{D} w(x,y) = \frac{P_0}{D}, \tag{4.1}$$

where the time-dependent term, $e^{j\omega t}$, has been dropped; $w(x,y)$ is the transverse displacement of the plate; D is the flexural rigidity and $D = Eh^3/12(1-\nu^2)$; E, ν, ρ and h are the Young's Modulus, Poisson's ratio, density and thickness of the plate, respectively; the net pressure on the plate, P_0, is uniform since the waveguide is assumed to have a subwavelength size and only the fundamental mode (plane wave) is allowed.

Since the plate is of arbitrary shape, the commonly used modal expansion method [106] is no longer suitable for solving Eq. (4.1). $w(x,y)$ can be represented as the sum of a homogeneous solution (w_h) and a particular solution (w_p), i.e. $w(x,y) = w(\vec{\mathbf{r}}) = w_h + w_p$; $\vec{\mathbf{r}}$ is the position vector of a point on the arbitrarily shaped plate. Substituting $w(\vec{\mathbf{r}})$ into Eq. (4.1), one can easily obtain that $w_p = -P_0/\rho h\omega^2$. The homogeneous solution (w_h) can be calculated by the meshless boundary method with radial basis functions (RBF) [111][112] for the free vibration of an arbitrarily shaped plate. The basic idea of the

meshless boundary method (simplified as the meshless method hereinafter) is that some discrete points along the boundary behave as source points to generate outward-spread circular flexural waves propagating in the plate which can be described by a general solution in terms of Bessel functions [111]. With all points along the boundary of the plate included, the net flexural displacement of a free vibrating plate can be obtained as w_h which is written as [111]

$$w_h(\vec{\mathbf{r}}) = \sum_{k=1}^{N} A_k \frac{1}{8\Lambda^2}\left[J_0\left(\Lambda\left|\vec{\mathbf{r}}_k - \vec{\mathbf{r}}\right|\right) + I_0\left(\Lambda\left|\vec{\mathbf{r}}_k - \vec{\mathbf{r}}\right|\right)\right] + \sum_{k=1}^{N} B_k \frac{1}{8\Lambda}\left[\frac{-J_1\left(\Lambda\left|\vec{\mathbf{r}}_k - \vec{\mathbf{r}}\right|\right) + I_1\left(\Lambda\left|\vec{\mathbf{r}}_k - \vec{\mathbf{r}}\right|\right)}{\left|\vec{\mathbf{r}}_k - \vec{\mathbf{r}}\right|}\right]\left\langle \vec{\mathbf{r}}_k - \vec{\mathbf{r}}\right\rangle\left\langle \vec{\mathbf{n}}_k \right\rangle, \tag{4.2}$$

where $\Lambda^4 = \rho h\omega^2 / D$; N is the total number of points along the boundary (edge points) of the arbitrarily shaped plate; J_m and I_m $(m = 0,1)$ denote the first kind of the mth order Bessel function and modified Bessel function, respectively; $\vec{\mathbf{r}}$ is the position vector of a collocation point on the arbitrarily shaped plate (including points along the boundary); $\vec{\mathbf{r}}_k$ is the position vector of the kth point on the boundary; $\vec{\mathbf{n}}_k$ is the outward normal unit vector of the kth point on the boundary; $\left|\vec{\mathbf{r}}_k - \vec{\mathbf{r}}\right|$ indicates the magnitude of the vector $\vec{\mathbf{r}} - \vec{\mathbf{r}}_k$; $\left\langle \vec{\mathbf{r}}_k - \vec{\mathbf{r}}\right\rangle\left\langle \vec{\mathbf{n}}_k \right\rangle$ is the dot product of vector $\vec{\mathbf{r}}_k - \vec{\mathbf{r}}$ and vector $\vec{\mathbf{n}}_k$; A_k and B_k are undetermined coefficients; when $\vec{\mathbf{r}}_k = \vec{\mathbf{r}}$, the second summation becomes zero because $\left\langle \vec{\mathbf{r}}_k - \vec{\mathbf{r}}\right\rangle\left\langle \vec{\mathbf{n}}_k \right\rangle = 0$;from this point forward, $\frac{1}{8\Lambda^2}\left[J_0\left(\Lambda\left|\vec{\mathbf{r}}_k - \vec{\mathbf{r}}\right|\right) + I_0\left(\Lambda\left|\vec{\mathbf{r}}_k - \vec{\mathbf{r}}\right|\right)\right]$ and

$\frac{1}{8\Lambda}\left[\frac{-J_1\left(\Lambda\left|\vec{\mathbf{r}}_k-\vec{\mathbf{r}}\right|\right)+I_1\left(\Lambda\left|\vec{\mathbf{r}}_k-\vec{\mathbf{r}}\right|\right)}{\left|\vec{\mathbf{r}}_k-\vec{\mathbf{r}}\right|}\right]\left\langle\vec{\mathbf{r}}_k-\vec{\mathbf{r}}\right\rangle\left\langle\vec{\mathbf{n}}_k\right\rangle$ are expressed symbolically by $C\left(\vec{\mathbf{r}},\vec{\mathbf{r}}_k\right)$ and $Q\left(\vec{\mathbf{r}},\vec{\mathbf{r}}_k\right)$, respectively, for simplification.

Applying the clamped boundary conditions (i.e. $w\left(\vec{\mathbf{r}}_i\right)=0$; $\partial w\left(\vec{\mathbf{r}}_i\right)/\partial\mathbf{n}_i=0$; i is the ith point on the boundary of the plate; $i=1,2\ldots N$), two equations can be produced

$$\begin{cases} w\left(\vec{\mathbf{r}}_i\right)=\sum_{k=1}^{N}A_kC\left(\vec{\mathbf{r}}_i,\vec{\mathbf{r}}_k\right)+\sum_{k=1}^{N}B_kQ\left(\vec{\mathbf{r}}_i,\vec{\mathbf{r}}_k\right)-\frac{P_0}{\rho h\omega^2}=0 \\ \frac{\partial w\left(\vec{\mathbf{r}}_i\right)}{\partial\mathbf{n}_i}=\sum_{k=1}^{N}A_k\frac{\partial C\left(\vec{\mathbf{r}}_i,\vec{\mathbf{r}}_k\right)}{\partial\mathbf{n}_i}+\sum_{k=1}^{N}B_k\frac{\partial Q\left(\vec{\mathbf{r}}_i,\vec{\mathbf{r}}_k\right)}{\partial\mathbf{n}_i}=0 \end{cases}, \tag{4.3}$$

where $\frac{\partial C\left(\vec{\mathbf{r}}_i,\vec{\mathbf{r}}_k\right)}{\partial\mathbf{n}_i}=\frac{1}{8\Lambda}\left[\frac{J_1\left(\Lambda\left|\vec{\mathbf{r}}_k-\vec{\mathbf{r}}_i\right|\right)-I_1\left(\Lambda\left|\vec{\mathbf{r}}_k-\vec{\mathbf{r}}_i\right|\right)}{\left|\vec{\mathbf{r}}_k-\vec{\mathbf{r}}_i\right|}\right]\left\langle\vec{\mathbf{r}}_k-\vec{\mathbf{r}}_i\right\rangle\left\langle\vec{\mathbf{n}}_i\right\rangle=C'\left(\vec{\mathbf{r}}_i,\vec{\mathbf{r}}_k\right)$;

$$\frac{\partial Q\left(\vec{\mathbf{r}}_i,\vec{\mathbf{r}}_k\right)}{\partial\mathbf{n}_i}=\frac{1}{8\Lambda}\left[-\frac{\Lambda\left\langle\vec{\mathbf{r}}_k-\vec{\mathbf{r}}_i\right\rangle\left\langle\vec{\mathbf{n}}_i\right\rangle\bullet\left\langle\vec{\mathbf{r}}_k-\vec{\mathbf{r}}_i\right\rangle\left\langle\vec{\mathbf{n}}_k\right\rangle}{\left|\vec{\mathbf{r}}_k-\vec{\mathbf{r}}_i\right|^2}\left(J_2\left(\Lambda\left|\vec{\mathbf{r}}_k-\vec{\mathbf{r}}_i\right|\right)+I_2\left(\Lambda\left|\vec{\mathbf{r}}_k-\vec{\mathbf{r}}_i\right|\right)\right)+\frac{\left\langle\vec{\mathbf{n}}_k\right\rangle\left\langle\vec{\mathbf{n}}_i\right\rangle}{\left|\vec{\mathbf{r}}_k-\vec{\mathbf{r}}_i\right|}\left(J_1\left(\Lambda\left|\vec{\mathbf{r}}_k-\vec{\mathbf{r}}_i\right|\right)-I_1\left(\Lambda\left|\vec{\mathbf{r}}_k-\vec{\mathbf{r}}_i\right|\right)\right)\right]$$

$=Q'\left(\vec{\mathbf{r}}_i,\vec{\mathbf{r}}_k\right)$.

Equation (4.3) can be further written in the matrix form as

$$\begin{pmatrix}\mathbb{C}_{N\times N} & \mathbb{Q}_{N\times N}\\ \mathbb{C}'_{N\times N} & \mathbb{Q}'_{N\times N}\end{pmatrix}\begin{pmatrix}A_{N\times 1}\\ B_{N\times 1}\end{pmatrix}=\frac{P_0}{\rho h\omega^2}\begin{pmatrix}1_{N\times 1}\\ 0_{N\times 1}\end{pmatrix}, \tag{4.4}$$

where $\mathbb{C}_{N\times N} = \begin{bmatrix} C(\vec{\mathbf{r}}_1,\vec{\mathbf{r}}_1) & C(\vec{\mathbf{r}}_1,\vec{\mathbf{r}}_2) & \cdots & C(\vec{\mathbf{r}}_1,\vec{\mathbf{r}}_N) \\ C(\vec{\mathbf{r}}_2,\vec{\mathbf{r}}_1) & C(\vec{\mathbf{r}}_2,\vec{\mathbf{r}}_2) & \cdots & C(\vec{\mathbf{r}}_2,\vec{\mathbf{r}}_N) \\ \vdots & \vdots & \ddots & \vdots \\ C(\vec{\mathbf{r}}_N,\vec{\mathbf{r}}_1) & C(\vec{\mathbf{r}}_N,\vec{\mathbf{r}}_2) & \cdots & C(\vec{\mathbf{r}}_N,\vec{\mathbf{r}}_N) \end{bmatrix}_{N\times N}$;

$\mathbb{Q}_{N\times N} = \begin{bmatrix} Q(\vec{\mathbf{r}}_1,\vec{\mathbf{r}}_1) & Q(\vec{\mathbf{r}}_1,\vec{\mathbf{r}}_2) & \cdots & Q(\vec{\mathbf{r}}_1,\vec{\mathbf{r}}_N) \\ Q(\vec{\mathbf{r}}_2,\vec{\mathbf{r}}_1) & Q(\vec{\mathbf{r}}_2,\vec{\mathbf{r}}_2) & \cdots & Q(\vec{\mathbf{r}}_2,\vec{\mathbf{r}}_N) \\ \vdots & \vdots & \ddots & \vdots \\ Q(\vec{\mathbf{r}}_N,\vec{\mathbf{r}}_1) & Q(\vec{\mathbf{r}}_N,\vec{\mathbf{r}}_2) & \cdots & Q(\vec{\mathbf{r}}_N,\vec{\mathbf{r}}_N) \end{bmatrix}_{N\times N}$;

$\mathbb{C}'_{N\times N} = \begin{bmatrix} C'(\vec{\mathbf{r}}_1,\vec{\mathbf{r}}_1) & C'(\vec{\mathbf{r}}_1,\vec{\mathbf{r}}_2) & \cdots & C'(\vec{\mathbf{r}}_1,\vec{\mathbf{r}}_N) \\ C'(\vec{\mathbf{r}}_2,\vec{\mathbf{r}}_1) & C'(\vec{\mathbf{r}}_2,\vec{\mathbf{r}}_2) & \cdots & C'(\vec{\mathbf{r}}_2,\vec{\mathbf{r}}_N) \\ \vdots & \vdots & \ddots & \vdots \\ C'(\vec{\mathbf{r}}_N,\vec{\mathbf{r}}_1) & C'(\vec{\mathbf{r}}_N,\vec{\mathbf{r}}_2) & \cdots & C'(\vec{\mathbf{r}}_N,\vec{\mathbf{r}}_N) \end{bmatrix}_{N\times N}$;

$\mathbb{Q}'_{N\times N} = \begin{bmatrix} Q'(\vec{\mathbf{r}}_1,\vec{\mathbf{r}}_1) & Q'(\vec{\mathbf{r}}_1,\vec{\mathbf{r}}_2) & \cdots & Q'(\vec{\mathbf{r}}_1,\vec{\mathbf{r}}_N) \\ Q'(\vec{\mathbf{r}}_2,\vec{\mathbf{r}}_1) & Q'(\vec{\mathbf{r}}_2,\vec{\mathbf{r}}_2) & \cdots & Q'(\vec{\mathbf{r}}_2,\vec{\mathbf{r}}_N) \\ \vdots & \vdots & \ddots & \vdots \\ Q'(\vec{\mathbf{r}}_N,\vec{\mathbf{r}}_1) & Q'(\vec{\mathbf{r}}_N,\vec{\mathbf{r}}_2) & \cdots & Q'(\vec{\mathbf{r}}_N,\vec{\mathbf{r}}_N) \end{bmatrix}_{N\times N}$; $A_{N\times 1} = \begin{bmatrix} A_1 \\ A_2 \\ \vdots \\ A_N \end{bmatrix}_{N\times 1}$; $B_{N\times 1} = \begin{bmatrix} B_1 \\ B_2 \\ \vdots \\ B_N \end{bmatrix}_{N\times 1}$;

$1_{N\times 1} = \begin{bmatrix} 1 \\ 1 \\ \vdots \\ 1 \end{bmatrix}_{N\times 1}$; $0_{N\times 1} = \begin{bmatrix} 0 \\ 0 \\ \vdots \\ 0 \end{bmatrix}_{N\times 1}$.

Undetermined $A_{N\times 1}$ and $B_{N\times 1}$ can be solved by multiplying $\begin{pmatrix} \mathbb{C}_{N\times N} & \mathbb{Q}_{N\times N} \\ \mathbb{C}'_{N\times N} & \mathbb{Q}'_{N\times N} \end{pmatrix}^{-1}$ on both sides of Eq. (4.4) and then the flexural displacement $w(\vec{\mathbf{r}})$ can be obtained as

$$w(\vec{\mathbf{r}}) = \sum_{k=1}^{N} A_k C(\vec{\mathbf{r}},\vec{\mathbf{r}}_k) + \sum_{k=1}^{N} B_k Q(\vec{\mathbf{r}},\vec{\mathbf{r}}_k) - \frac{P_0}{\rho h \omega^2}, \tag{4.5}$$

4.1.2 Acoustic impedance and effective density

With the flexural displacement $w(\vec{\mathbf{r}})$ solved from Eq. (4.5), the acoustic impedance Z_{am} of a vibrating plate can be calculated by

$$Z_{am} = \frac{P_0}{j\omega \bar{w} S}, \tag{4.6}$$

where S is the area of an arbitrarily shaped plate; $\bar{w}$ is the average flexural displacement which can be obtained from Eq. (4.5) and is proportional to P_0 so that eventually Z_{am} is independent of P_0.

Once Z_{am} is obtained, the effective density (ρ_{eff}) of the plate-type AMM can be obtained using a lumped model and reads [1][28]

$$\rho_{eff} = \frac{\left(j\omega M_a + Z_{am} \right) S}{j\omega d}, \tag{4.7}$$

where M_a is the acoustic mass of the air medium in the waveguide and is equal to $\rho_0 d/S$; ρ_0 is the air density; d is the length of the unit cell assuming the thickness of the plate is negligible. Otherwise the length of the unit cell is $d+h$.

4.2 Simulation results

To verify the effective density calculated from the meshless method described in section II, the acoustic impedances and effective densities of plate-type AMMs with

circular, triangular, and hexagonal plates are calculated using the meshless method and FEM simulation (COMSOL: acoustic-solid interaction module). Results are shown in the following three subsections separately. In all cases, the material properties of plates are identical ($E = 10MPa$, $v = 0.49$, $\rho = 1000\,kg/m^3$) and the thickness of plates (h) and length of one unit cell (d) are 0.1*mm* and 2*mm*, respectively. Based on the finite-difference approximation method [27][28][5][108], the effective density can be extracted from the FEM simulation as [28]

$$\rho_{eff} = \frac{\Delta p}{d}\frac{j}{\omega \bar{V}} \tag{4.8}$$

where $\Delta p = p_1 - p_2$; p_1 and p_2 are the pressures at the right end and left end of the unit cell, respectively; $\bar{V}$ is the average transverse velocity on the plate. This extracted effective density can be then compared with the one predicted by the proposed method that involves the meshless method and lumped model.

4.2.1 Circular plate-type AMMs

A fully clamped circular plate with diameter =10 *mm* is first considered. As shown by Fig. 4.1(c), a number of edge points and collocation points distributed on the circle are used to implement the meshless method. Since different numbers of edge points and collocation points (in other words, the spacing between two collocation points) can affect the accuracy of the calculation, their relation with the numerical error should be investigated. Figure 4.1(b) shows the error of effective density which is calculated as

$error_{\rho_{eff}} = abs\left[\left(\rho_{eff\_meshless\_method} - \rho_{eff\_analytical}\right)/\rho_{eff\_analytical}\right] \times 100\%$ at 220 *Hz*. $\rho_{eff\_analytical}$ can be obtained by applying the analytical solution of the acoustic impedance of a fully clamped circular plate (Z_{am_circle}) in the lumped model (Eq. (4.7)). Z_{am_circle} reads [1]

$$Z_{am\_circle} = \frac{-j\omega\rho h}{S} \frac{I_1(k_m r) J_0(k_m r) + J_1(k_m r) I_0(k_m r)}{I_1(k_m r) J_2(k_m r) - J_1(k_m r) I_2(k_m r)} \tag{4.9}$$

where $k_m = \left(\omega\sqrt{\frac{\rho h S}{D}}\right)^{1/2}$ and r is the radius of the circular plate.

Although Fig. 4.1(b) does not show a strictly monotonous decline of the error as the number of edge points increase or as the spacing between two collocation points reduce, the error is contained under 1% once reasonable numbers of edge points and collocation point spacing are reached (e.g., 10 edge points and 0.2 mm spacing). Based on the error shown in Fig. 4.1(b), the number of edge points and spacing along x (or y) direction between each two collocation points are chosen as 10 and $0.067mm$, respectively, in order to obtain a result with an error under 0.1%. Correspondingly, there are 17661 collocation points in total. Figure 4.1(c) demonstrates how the 10 edge points (black thick dots) and 17661 collocation points (blue small dots) are distributed on the circle, and the directions of normal unit vectors on each edge point. These collocation points are uniformly distributed in the interior of the circle. Figure 4.1(a) shows the FEM setup with a circular plate clamped in a circular waveguide. Substituting corresponding normal unit vectors, edge point, and collocation point positions into Eq. (4.5), the flexural displacement of the circular plate can be obtained and the corresponding Z_{am} of the plate can be subsequently calculated from Eq. (4.6).

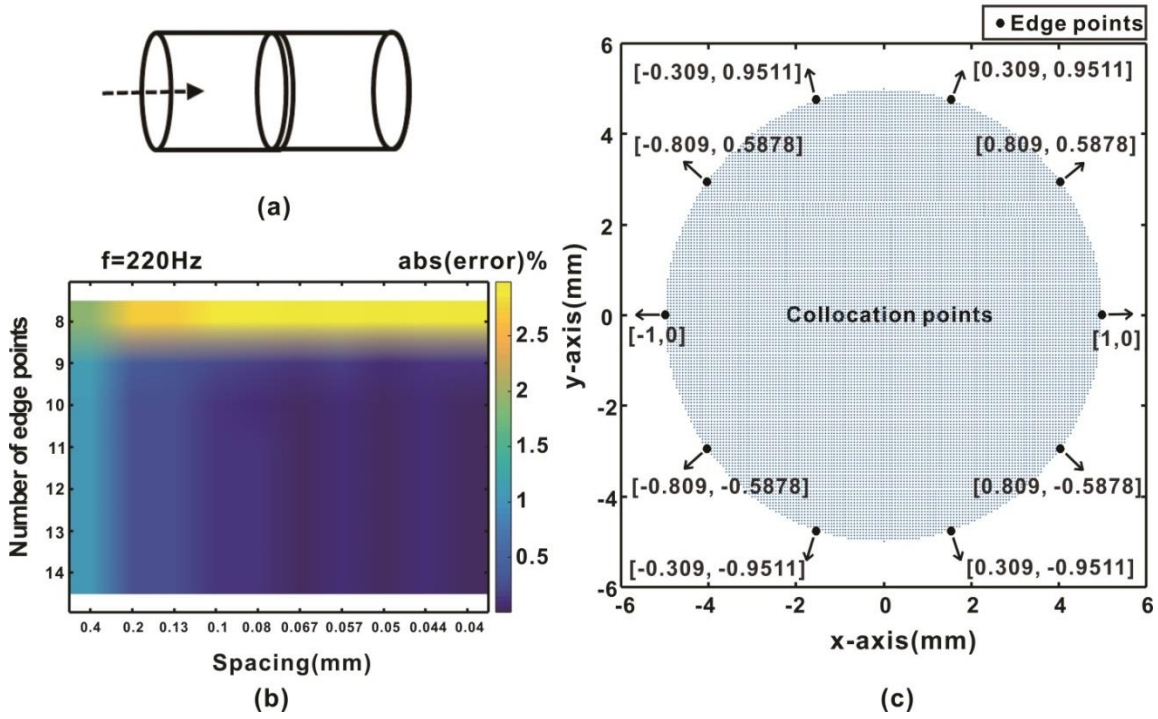

Figure 4.1. (a) A fully-clamped circular plate within a 1-D waveguide; the dash arrow represents the incident plan wave. (b) The error of the effective density under different numbers of edge points and different spacings between collocation points. (c) The selected edge points (block thick dots), collocation points (blue dense dots), and the normal unit vectors on each edge point (arrows and brackets with numbers).

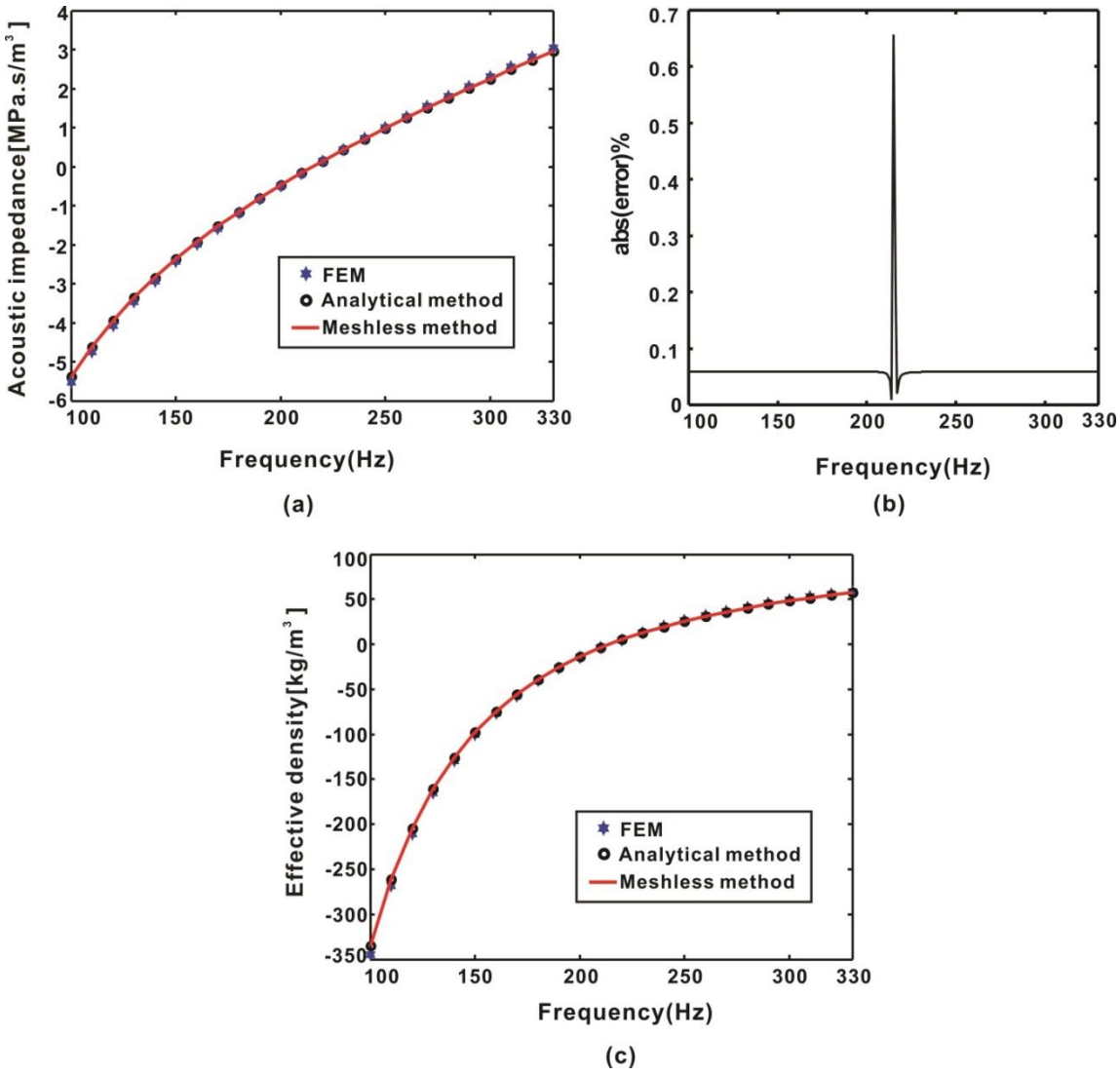

Figure 4.2. (a) The acoustic impedances of a fully-clamped circular plate from the FEM, analytical solution, and meshless method. (b) The error of Z_{am} produced by the meshless method. (c) The effective densities calculated from different models.

The comparison among different methods is depicted in Fig. 4.2. Based on the plot of the acoustic impedance (Fig. 4.2(a)), the first resonance frequency of the plate can be determined (around 220 *Hz*) by identifying where zero acoustic impedance occurs. This

agrees with the analytical solution of the first resonance frequency for a circular plate as [1]

$$f_{r1} = 1.6259 \frac{1}{r^2} \sqrt{\frac{D}{\rho h}} = 215.37 Hz \tag{4.10}$$

Since the analytical Z_{am} of a fully-clamped circular plate is well-known [1][113], comparing the result from the meshless method with analytical solution can help us examine how accurate the meshless method is. Figure 4.2(a) shows that the Z_{am} predicted from the meshless method matches well with the analytical solution and FEM results. Only the imaginary part of Z_{am} is shown because the real part (resistance part) is zero. The error between the analytical solution and the meshless method is calculated by $error_{Z_{am}} = abs\left[\left(Z_{\text{am\_}meshless\_method} - Z_{\text{am\_}analytical}\right)/Z_{\text{am\_}analytical}\right] \times 100\%$ and is shown in Fig. 4.2(b). Except at the resonance frequency, where the error peaks, the error elsewhere is in general very small. Effective densities from different models are then calculated from Eqs. (4.7) and (4.8) and good agreement can be seen in Fig. 4.2(c). Below the first resonance frequency of the plate, the broadband negative ρ_{eff} is clearly generated.

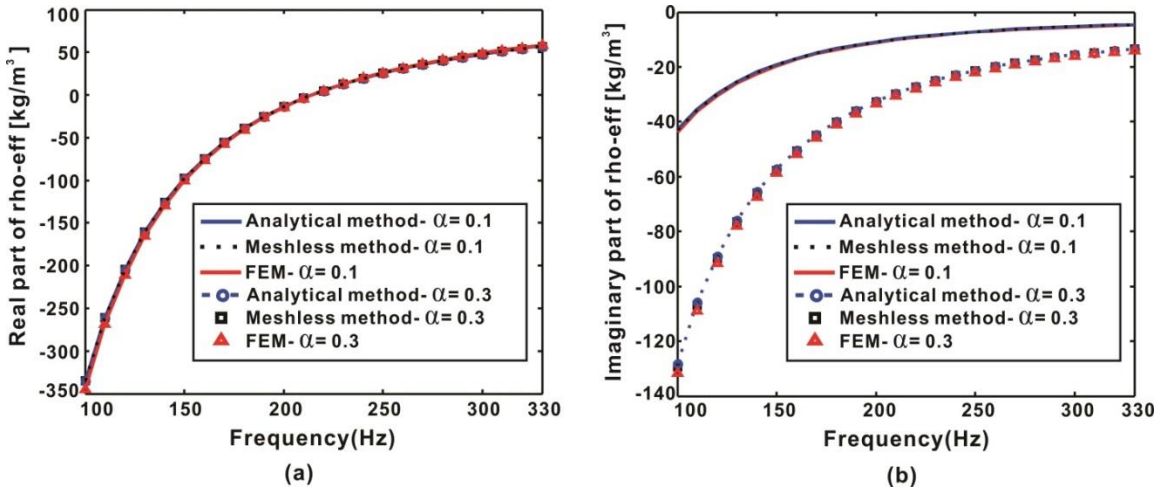

Figure 4.3. The effect of the loss factor α on the effective density of the circular plate-type AMM. α is chosen as 0.1 and 0.3. (a) Real part of the effective density. (b) Imaginary part of the effective density.

To further verify the meshless method, the damping of the plate is taken into account by considering a loss factor α to form a complex Young's modulus, i.e. $E' = E(1+ j\alpha)$. α is considered as 0.1 and 0.3 and the effective density becomes a complex number as shown in Fig. 4.3. All results agree excellently and the unchanged real part of the effective density and loss-introduced negative imaginary part of the effective density follow the expectations [28].

4.2.2 Triangular plate-type AMMs

A fully clamped triangular plate with length of each side =10*mm* is considered next. Similar to the procedure done in the circular case, the spacing between each two collocation points along x (or y) direction and the number of edge points are $0.067mm$ and 18, respectively, which lead to results with reasonably small errors. The edge points, collocation points (there are 9818 collocation points in total), and normal unit vectors on edge points were generated first as shown in Fig. 4.4 and then plugged into Eqs. (4.4)-(4.7) to solve for Z_{am} and ρ_{eff}. It should be pointed out that the normal unit vector at each vertex is the average unit vector from the two normal unit vectors of the two adjacent edge points. From the plot of acoustic impedance (Fig. 4.5(a)), the first resonance frequency can be determined and is around 520 *Hz* (From FEM, the first resonance frequency is estimated to be around 536 *Hz*).

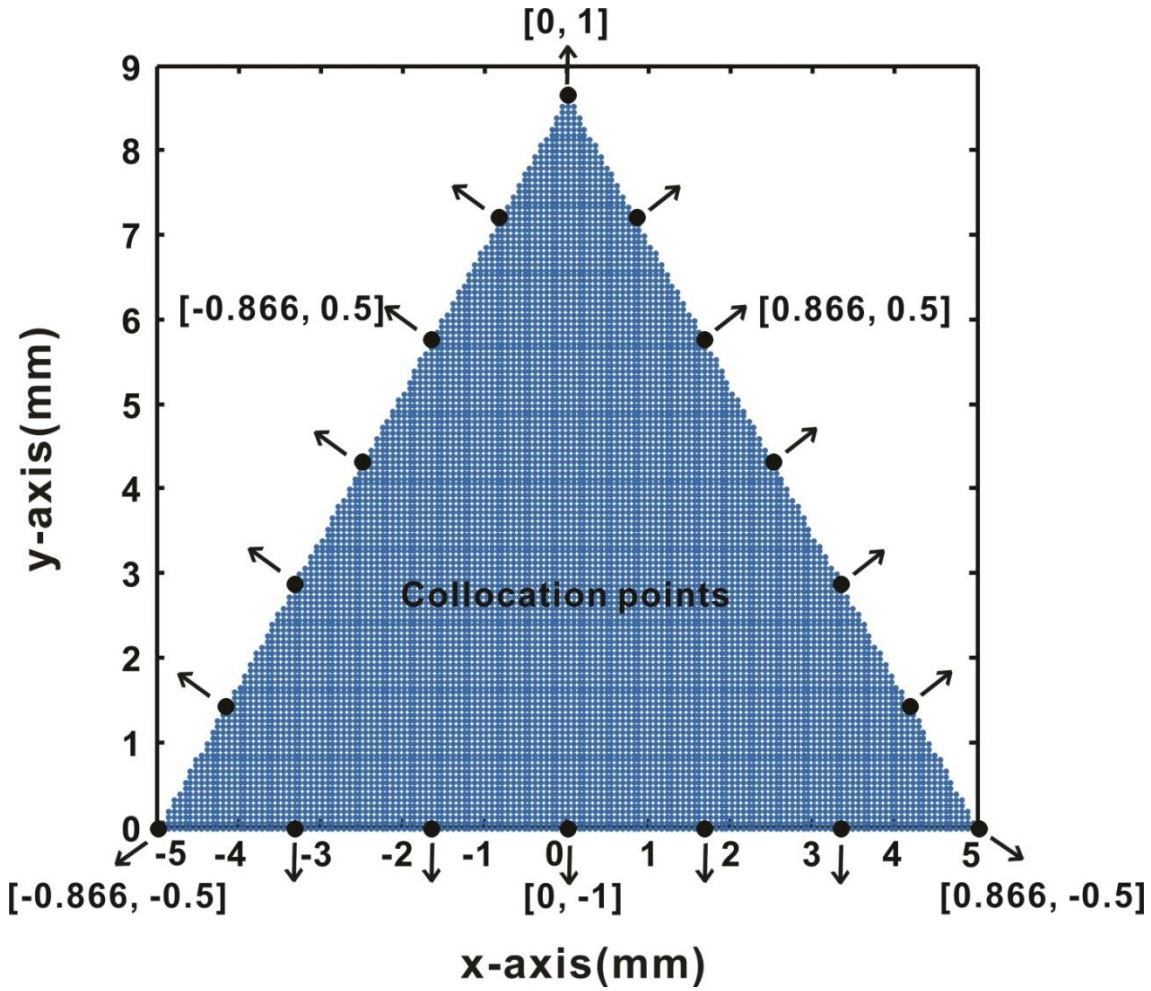

Figure 4.4. The selected edge points (block thick dots), collocation points (blue dense dots), and the normal unit vectors on each edge point (arrows and brackets with numbers) for a triangular plate.

Furthermore, as shown in Figs. 4.5 and 4.6, the meshless method is in good agreement with FEM for predicting the acoustic impedance and effective density (with and without the loss). However, some appreciable errors are found in the low-frequency region (below the first resonance frequency of the plate). This might have been because

the triangle has sharp corners so that inaccurate average normal unit vectors on vertexes are generated. These inaccurate normal unit vectors contribute to the second summation (with coefficient B_k) on the right hand side of Eq. (4.2) and this inaccuracy is amplified at low frequencies due to the fact that the second summation is inversely proportional to Λ and $\Lambda^4 = \rho h \omega^2 / D$. If sharp corners are replaced by smoother ones, more accurate average normal unit vectors can be obtained and this low-frequency discrepancy could potentially be reduced. However, this smoothing process could also introduce another error since the shape is slightly changed.

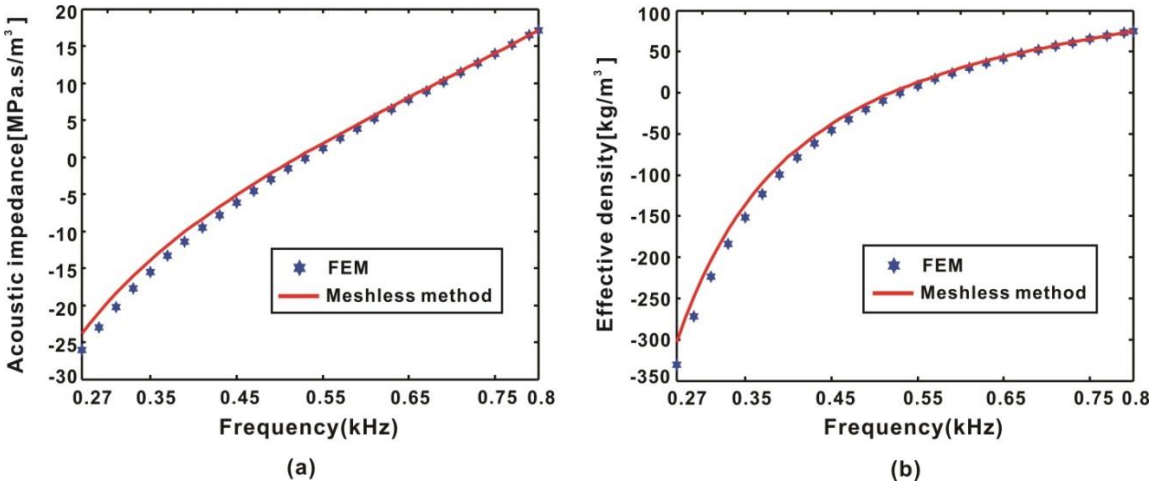

Figure 4.5. (a) The acoustic impedances of a fully-clamped triangle plate from the FEM and meshless method. (b) The effective densities from different models.

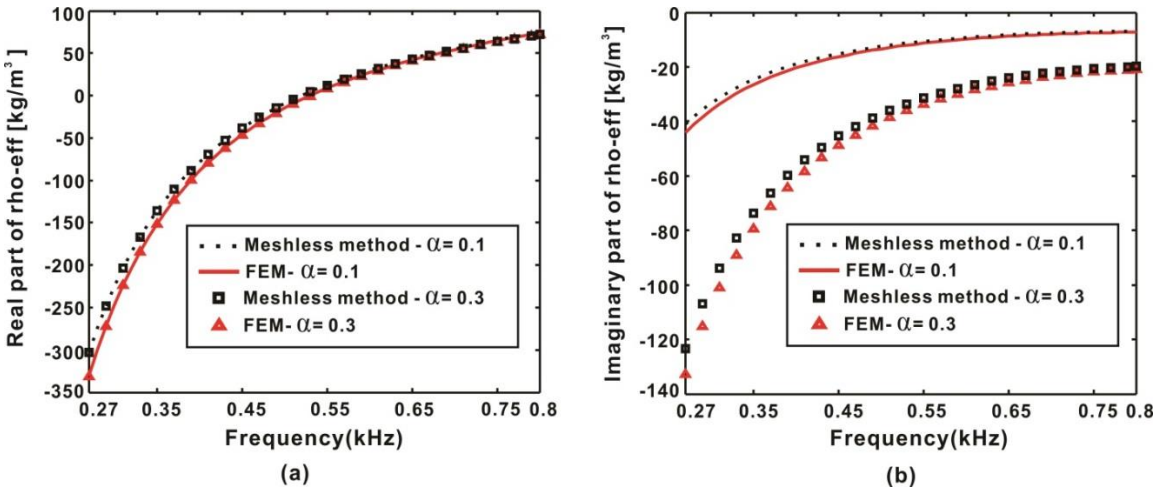

Figure 4.6. The effect of the loss factor α on the effective density of the triangle plate-type AMM. α is chosen as 0.1 and 0.3. (a) Real part of the effective density. (b) Imaginary part of the effective density.

4.2.3 Hexagonal plate-type AMMs

Finally, a fully-clamped hexagonal plate with length of each side =10*mm* is considered. The spacing between each two collocation points along x (or y) direction and the number of edge points are chosen as $0.1155mm$ ($0.133mm$) and 42, respectively. As can be seen, the spacing between collocations points are different in x and y directions in this case. The edge points, collocation points (there are 16971 collocation points in total), and normal unit vectors on edge points were generated first as shown in Fig. 4.7. Following the similar procedures in the circular and triangular cases, corresponding results can be obtained and good agreements of the acoustic impedance and effective density can be seen in Fig. 4.8. The first resonance frequency of this plate can be determined to be around 70 *Hz* (From FEM, the first resonance frequency is estimated to be around 68 *Hz*).

Figure 4.9 shows that the effect of damping can be taken into account in the meshless method for the hexagonal case. The hexagonal case has better results than the triangular one in the low frequency region, because the corners are less sharp (angles are smaller).

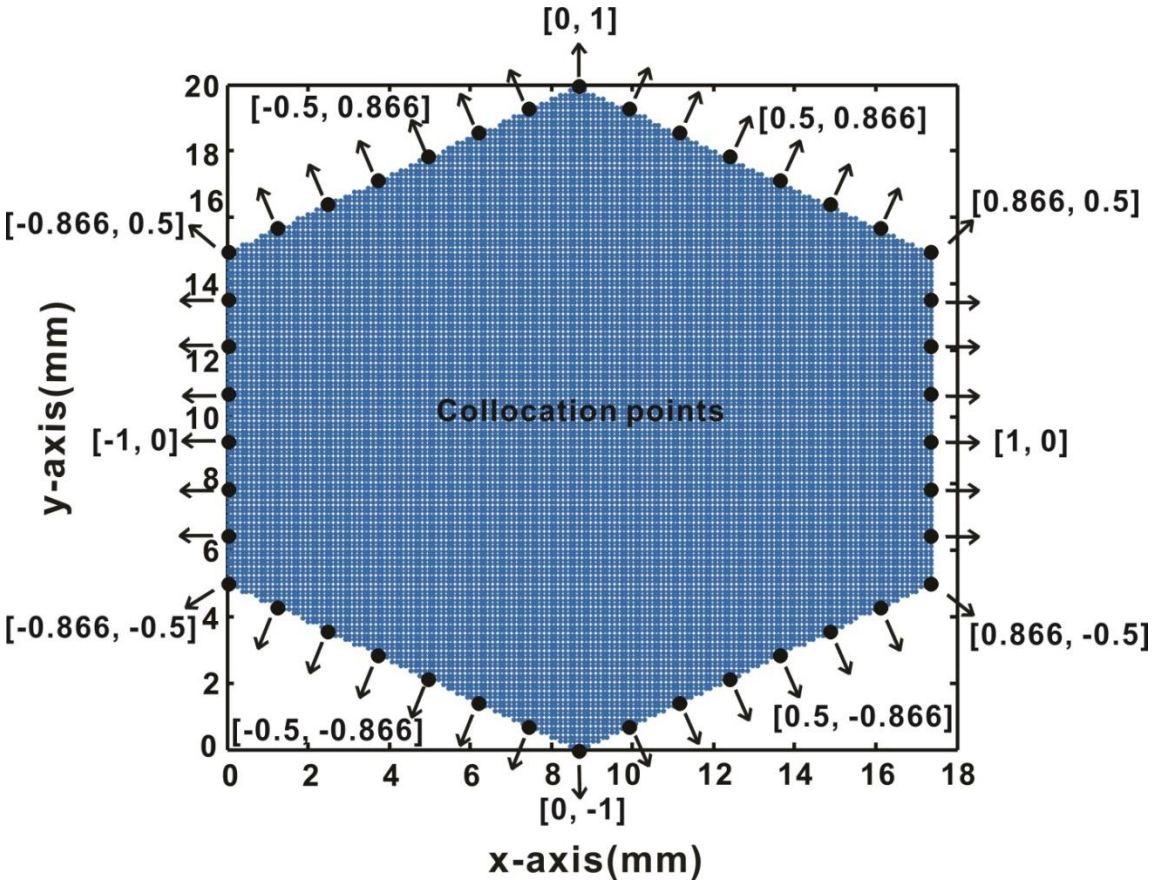

Figure 4.7. The selected edge points (block thick dots), collocation points (blue dense dots), and the normal unit vectors on each edge point (arrows and brackets with numbers) for a hexagonal plate.

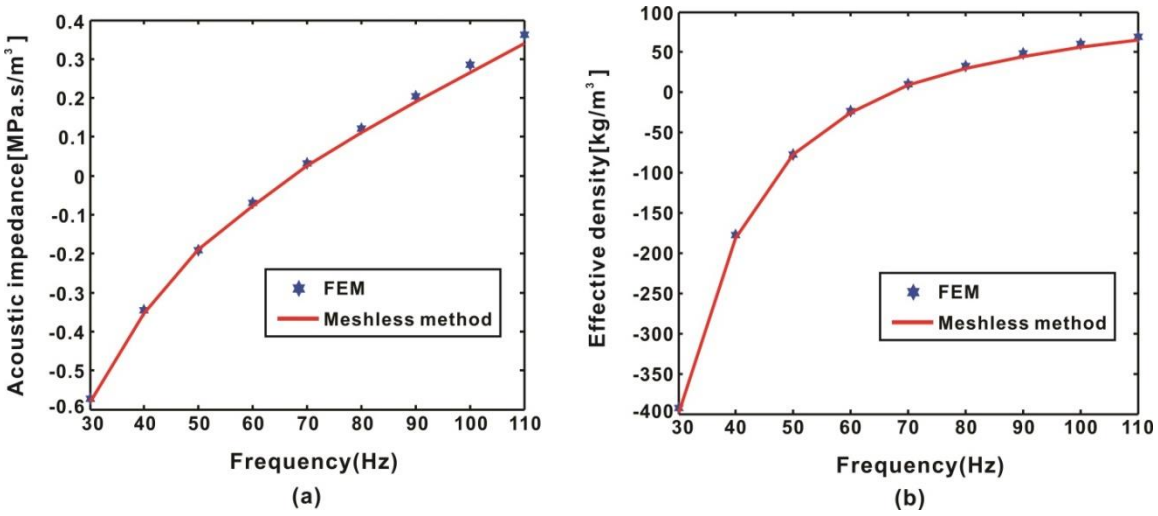

Figure 4.8. (a) The acoustic impedances of a fully-clamped hexagonal plate from the FEM and meshless method. (b) The effective densities from different models.

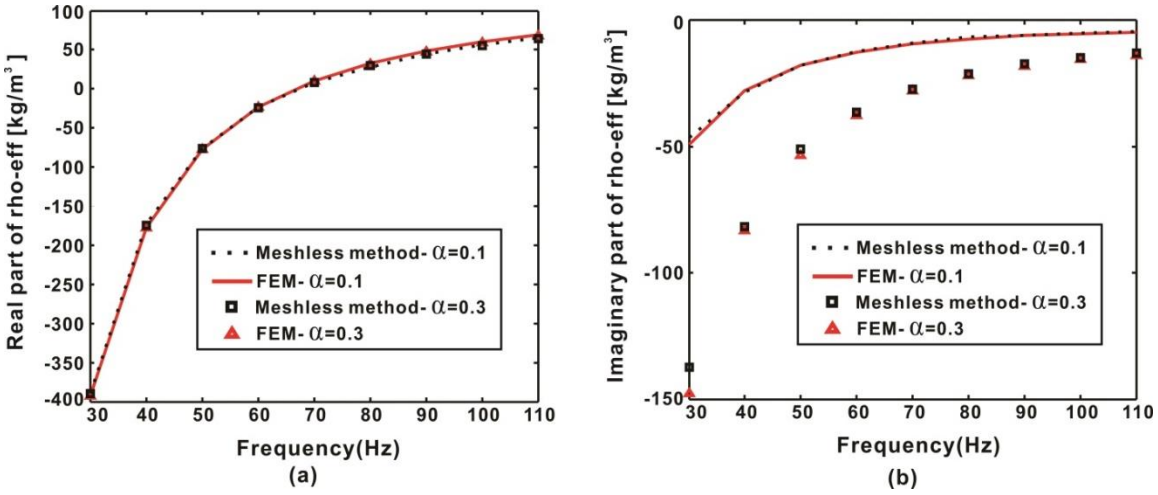

Figure 4.9. The effect of the loss factor α on the effective density of the hexagonal plate-type AMM. α is chosen as 0.1 and 0.3. (a) Real part of the effective density. (b) Imaginary part of the effective density.

4.3 Summary

This chapter demonstrates that the meshless method is capable of evaluating effective densities of arbitrarily shaped plate-type AMMs without mass attached. Plates with three different shapes with or without damping are considered to validate the meshless method. Good agreements are found among circular and hexagonal cases when evaluating the acoustic impedance and effective density. In the case of triangular plate, some errors in the low frequency region are observed and they are possibly due to the sharp corners of the triangle. In addition, since the effective density is close to zero around the first resonance frequency, the accurate prediction of this frequency makes this method suitable for designing density-near-zero AMMs. The framework presented here not only can be applied to different applications having plates in non-circular or non-rectangular shapes (like honeycomb structure [30]) but it also provides a new pathway to tune the effective density of plate-type AMMs without mass attached.

Chapter V

Investigation of the Fluid Loading Effect on Plate-type Acoustic Metamaterials

Most applications of AMMs interact with air medium (as mentioned in Chapters I and II), but these ideas also can be extended to applications that interact with fluid (i.e., water). The design of complimentary metamaterials (CMMs) [5] is one of AMMs' applications to deal with water medium. The design has the potential to improve the resolution of medical ultrasound imaging and medical ultrasound treatment (for example, by breaking up a kidney stone).

Subwavelength imaging [31][32] and cloaking [33] potentially can be extended to the underwater version to improve the medical ultrasound imaging and achieve 2D underwater cloaking (Zhang *et al.* have developed a non-plate-type AMMs for 2D underwater cloaking [114]), respectively. Since heavy medium causes non-ignorable reaction forces on the plate of plate-type AMMs, the behavior of effective density of AMMs under water is significantly different from that experienced in air.

The aim of this chapter is to develop an analytical model to include the medium effect in evaluating the effective densities of plate-type AMMs. The waveguide theory is utilized to obtain the reaction pressure from medium and then the corresponding acoustic impedance of plate can be calculated. Following the similar procedure in Chapters III and IV, the effective density can be evaluated by a lumped model. An FEM model is then applied to verify the solidity of this analytical model.

5.1 Medium effect on the plate-type AMMs without mass attached

5.1.1 Reaction pressure from medium in a waveguide

For a fully clamped rectangular thin plate under a net sound pressure $P_{net}(x,y)$, the governing equation of the transverse displacement $w(x,y)$ can be read as

$$\nabla^4 w(x,y) - \frac{\rho h \omega^2}{D} w(x,y) = \frac{P_{net}(x,y)}{D}, \tag{5.1}$$

where $w(x,y)$ is the spatial term of the transverse displacement on the plate; ω is the angular frequency of harmonic excitations; the time-dependent term, that is, $e^{j\omega t}$, has been dropped through the whole equation; D is the flexural rigidity and $D = Eh^3 / 12(1-v^2)$; and E, v, ρ, and h are the Young's Modulus, Poisson's ratio, density, and thickness of the plate, respectively.

Consider that this plate is clamped in a subwavelength waveguide, and the fluid loading on both sides of the plate also is taken into account. Then the net pressure $P_{net}(x,y)$ in Eq. (5.1) can be decomposed as the sum of the excitation pressure ($P_i(x,y)$ is the sum of the input pressure and the reflected pressure in the incident domain [115]) and the reaction pressure from medium ($P_{reaction}(x,y)$), i.e. $P_{net}(x,y) = P_i(x,y) + P_{reaction}(x,y)|z=0$. Because of the subwavelength scale of the waveguide, the excitation pressure is a plane wave ($P_i(x,y) = P_i$) under a range of operational frequencies around the first resonance frequency of the plate.

Based on the acoustic waveguide theory, the vibration of a plate inside a rectangular waveguide is a sound source and generates the radiated sound pressure field in the transmitted domain ($P_{Rt}(x,y,z)$) and incident domain ($P_{Ri}(x,y,z)$), which can be solved by the variable separation method in the three-dimensional (3D) wave equation with sound hard boundary (normal vibrating velocity is zero) on the boundaries of x- and y-directions and expressed as [116]

$$P_{Rt}(x,y,z)=\sum_{p=0}^{\infty}\sum_{q=0}^{\infty}A_{pq}\cos\left(\frac{p\pi x}{l_x}\right)\cos\left(\frac{q\pi y}{l_y}\right)e^{-jk_z z},$$

$$P_{Ri}(x,y,z)=\sum_{p=0}^{\infty}\sum_{q=0}^{\infty}A_{pq}\cos\left(\frac{p\pi x}{l_x}\right)\cos\left(\frac{q\pi y}{l_y}\right)e^{jk_z z}, \tag{5.2}$$

where the origin of z-axis is at plate and the positive z direction is along the propagation of the incident plane wave (refer to Fig. 3.1(a)); *p* and *q* are propagation modal numbers along *x* and *y* direction, respectively; double summations include all radiated sound pressure modes in waveguides; l_x and l_y are the dimensions of the plate along *x* and *y* directions, respectively; $k_z=\sqrt{(\omega/c_0)^2-\left[(p\pi/l_x)^2+(q\pi/l_y)^2\right]}$ is the wavenumber along *z* direction; $A_{pq}=\frac{E_{pq}\omega^2\rho_0 j}{l_x l_y k_z}\int_0^{l_x}\int_0^{l_y}w(x,y)\phi_p(x)\phi_q(y)dxdy$; when $p=q=0$, $E_{pq}=1$; when $p=0$, $q\neq 0$ or $p\neq 0$, $q=0$, $E_{pq}=2$; when $p\neq 0$ and $q\neq 0$, $E_{pq}=4$; and for simplification, $\cos\left(\frac{p\pi x}{l_x}\right)=\phi_p(x)$, $\cos\left(\frac{q\pi y}{l_y}\right)=\phi_q(y)$, and $C_{pq}=\frac{E_{pq}\omega^2\rho_0 j}{l_x l_y k_z}$ in the following contents.

By setting $z=0$ in Eq. (5.2), the resultant radiated pressure from the plate on the adjacent medium is equal to $P_{Rt}(x,y,0)+P_{Ri}(x,y,0)=2\sum_{p=0}^{\infty}\sum_{q=0}^{\infty}A_{pq}\phi_p(x)\phi_q(y)$. This is a result of the anti-symmetric pressure fields of two sides with respect to the plate. The resultant reaction pressure from adjacent medium on the plate, $P_{reaction}(x,y)$, has the same magnitude as the resultant radiated pressure. Therefore, the $P_{net}(x,y)$ can be obtained as

$$P_{net}(x,y)=P_i+2\sum_{p=0}^{\infty}\sum_{q=0}^{\infty}A_{pq}\phi_p(x)\phi_q(y). \tag{5.3}$$

$w(x,y)$ can be expanded by eigenfunctions as

$$w(x,y)=\sum_{m=1}^{\infty}\sum_{n=1}^{\infty}w_{mn}X_m(x)Y_n(y), \tag{5.4}$$

where $X_m(x)$ and $Y_n(y)$ can be found in Eq. (3.4).

Combining Eqs. (5.1)-(5.4) and then multiplying each term by eigenfunctions with different modal numbers, i.e. $X_r(x)Y_s(y)$, and integrating over the whole plate, Eq. (5.1) can be rewritten as

$$Dw_{rs}\left(I_1I_2+2I_3I_4+I_5I_6\right)-\rho h\omega^2 w_{rs}I_2I_6=\int_0^{l_x}\int_0^{l_y}P_iX_rY_s\,dxdy$$

$$+2\sum_{p=0}^{\infty}\sum_{q=0}^{\infty}C_{pq}\int_0^{l_x}\int_0^{l_y}\left[\int_0^{l_x}\int_0^{l_y}\sum_{m=1}^{\infty}\sum_{n=1}^{\infty}w_{mn}X_mY_n\phi_p\phi_q\,dxdy\right]\phi_p\phi_qX_rY_s\,dxdy, \tag{5.5}$$

where

$I_1 = \int_0^{l_x} X_m^{(4)} X_m dx$, $I_2 = \int_0^{l_y} Y_n^2 dy$, $I_3 = \int_0^{l_x} X_m'' X_m dx$, $I_4 = \int_0^{l_y} Y_n'' Y_n dy$, $I_5 = \int_0^{l_y} Y_n^{(4)} Y_n dy$, $I_6 = \int_0^{l_x} X_m{}^2 dx$ and the superscript in "()" indicates the order of the derivative and double prime is the second order derivative; the summation term in the right-hand side of this equation can be rewritten as $2\sum_{m=1}^{\infty}\sum_{n=1}^{\infty} w_{mn} \sum_{p=0}^{\infty}\sum_{q=0}^{\infty} C_{pq} \int_0^{l_x} X_m \phi_p dx \int_0^{l_y} Y_n \phi_q dy \int_0^{l_x} X_r \phi_p dx \int_0^{l_y} Y_s \phi_q dy$ and then simplified as $2\sum_{m=1}^{\infty}\sum_{n=1}^{\infty} w_{mn} \sum_{p=0}^{\infty}\sum_{q=0}^{\infty} C_{pq} B_{pq,mn} B_{pq,\mathrm{rs}} = 2\sum_{m=1}^{\infty}\sum_{n=1}^{\infty} w_{mn} C_{mnrs}$, in which $B_{pq,mn} = \int_0^{l_x} X_m \phi_p dx \int_0^{l_y} Y_n \phi_q dy$ and $B_{pq,\mathrm{rs}} = \int_0^{l_x} X_r \phi_p dx \int_0^{l_y} Y_s \phi_q dy$.

From Eq. (5.5), w_{rs} then can be simply represented as

$$w_{rs} = E_{1,rs} + E_{2,rs} \sum_{m=1}^{\infty}\sum_{n=1}^{\infty} w_{mn} C_{mnrs} , \tag{5.6}$$

where $E_{1,rs} = \dfrac{\int_0^{l_x}\int_0^{l_y} P_i X_r Y_s dxdy}{D\left(I_1 I_2 + 2I_3 I_4 + I_5 I_6\right) - \rho h \omega^2 I_2 I_6}$ and

$E_{2,rs} = \dfrac{2}{D\left(I_1 I_2 + 2I_3 I_4 + I_5 I_6\right) - \rho h \omega^2 I_2 I_6}$.

w_{rs} cannot be solved individually, but it can be solved in a series of equations (list equations with different modal numbers). To solve w_{rs} , Eq. (5.6) is rearranged in the matrix form as

$$\begin{bmatrix} w_{11} \\ w_{12} \\ \vdots \\ w_{1N} \\ w_{21} \\ w_{22} \\ \vdots \\ w_{2N} \\ \vdots \\ w_{NN} \end{bmatrix}_{N^2\times 1} = \left[E_{1,rs}\right]_{N^2\times 1} + \left[E_{2,rs}\right]_{N^2\times N^2}\left[C_{mnrs}\right]_{N^2\times N^2} \begin{bmatrix} w_{11} \\ w_{12} \\ \vdots \\ w_{1N} \\ w_{21} \\ w_{22} \\ \vdots \\ w_{2N} \\ \vdots \\ w_{NN} \end{bmatrix}_{N^2\times 1} \tag{5.7}$$

where

$$\left[E_{1,rs}\right]_{N^2\times 1} = \begin{bmatrix} E_{1,11} \\ E_{1,12} \\ \vdots \\ E_{1,NN} \end{bmatrix}_{N^2\times 1} \quad ; \quad \left[E_{2,rs}\right]_{N^2\times N^2} = \begin{bmatrix} E_{2,11} & 0 & \cdots & 0 \\ 0 & E_{2,12} & \ddots & \vdots \\ \vdots & \ddots & \ddots & 0 \\ 0 & \cdots & 0 & E_{2,NN} \end{bmatrix}_{N^2\times N^2} \quad ;$$

$$\left[C_{mnrs}\right]_{N^2\times N^2} = \begin{bmatrix} C_{1111} & C_{1211} & \cdots & C_{NN11} \\ C_{1112} & C_{1212} & \cdots & C_{NN12} \\ \vdots & \vdots & \ddots & \vdots \\ C_{11NN} & C_{12NN} & \cdots & C_{NNNN} \end{bmatrix}_{N^2\times N^2}$$; and N is the upper limit of double summations (ideally $N=\infty$, but it is sufficient to apply a limited value for N to obtain a converged result).

The Eq. (5.7) can be further arranged, and then the matrix of w_{rs} can be solved as

$$\begin{bmatrix} w_{11} \\ w_{12} \\ \vdots \\ w_{1N} \\ w_{21} \\ w_{22} \\ \vdots \\ w_{2N} \\ \vdots \\ w_{NN} \end{bmatrix}_{N^2\times 1} = \left\{ [1]_{N^2\times N^2} - \left[E_{2,rs}\right]_{N^2\times 1} \left[C_{mnrs}\right]_{N^2\times N^2} \right\}^{-1} \left[E_{1,rs}\right]_{N^2\times 1}, \tag{5.8}$$

where $[1]_{N^2\times N^2}$ is $N^2 \times N^2$ identity matrix. After applying the result of $w_{rs}\,(=w_{mn})$ into Eq. (5.4), the flexural displacement of the plate, $w(x,y)$, in a rectangular waveguide with consideration of medium effect can be obtained.

5.1.2 Acoustic impedance and effective density

With the flexural displacement $w(x,y)$ solved in the previous subsection, the acoustic impedance Z_{am} of the vibrating plate can be calculated as

$$Z_{am} = \frac{\int_0^{l_x}\int_0^{l_y} P_{net}(x,y)\,dxdy}{j\omega\bar{w}S^2}, \tag{5.9}$$

where S is the area of a arbitrarily shaped plate, and $\bar{w}$ is the average flexural displacement, which can be obtained from Eqs. (5.4) and (5.8).

Substituting Eq. (5.3) into Eq. (5.9), Eq. (5.9) becomes

$$Z_{am} = \frac{P_i S + 2\sum_{p=0}^{\infty}\sum_{q=0}^{\infty} C_{pq} \sum_{m=1}^{\infty}\sum_{n=1}^{\infty} w_{mn} B_{pq,mn} \int_0^{l_x} \phi_p(x)dx \int_0^{l_y} \phi_q(y)dy}{j\omega \bar{w} S^2}. \quad (5.10)$$

Once Z_{am} is obtained, the effective density (ρ_{eff}) of a waveguide unit can be obtained [1] [28] as

$$\rho_{eff} = \frac{(j\omega M_a + Z_{am})S}{j\omega d}, \quad (5.11)$$

where M_a is the acoustic mass of the medium in waveguide and is equal to $\rho_0 d/S$; ρ_0 is the medium density; and d is the length of a unit cell, assuming the thickness of the plate is negligible. Otherwise, the length of the unit cell is $d+h$.

5.2 Effective densities of AMMs without mass attached under air and water mediums

To verify the analytical model derived in Section 5.1, consider an aluminum plate ($E = 70GPa$, $v = 0.33$ and $\rho = 2700 kg/m^3$) with dimensions $l_x = l_y = 10mm$ and thickness $h = 0.1mm$ as a fully-clamped plate in rectangular waveguides with air (air density $\rho_{air} = 1.2 kg/m^3$; speed of sound in air $C_{air} = 343 m/s$) and water (water density $\rho_{water} = 1000 kg/m^3$; speed of sound in air $C_{water} = 1481 m/s$) mediums in an analytical model and a FEM model. Figure 5.1 shows the acoustic impedances of the plate and the effective densities of the AMM with the air medium obtained from the FEM model, analytical model (including medium effect), and analytical model without medium effect

(which is the same as the analytical model in Chapter III or set A_{pq} in Eqs. (5.2) and (5.3) equal to zero) match well. This result shows that since the air medium is so light compared with the density of the plate that the reaction pressure from the air medium can be ignored. The first resonance frequency of the plate is around 8900 *Hz* (for both FEM and analytical model) and the effective density is close to zero around this frequency.

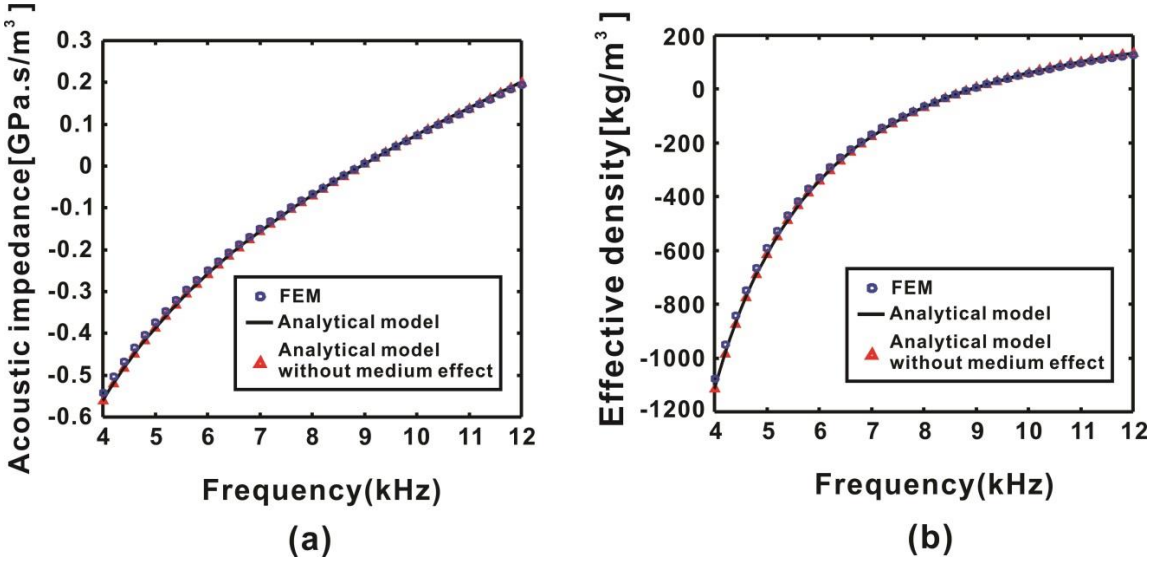

Figure 5.1. (a) The acoustic impedances of a fully-clamped square plate surrounded by the air medium from the FEM model, analytical model, and analytical model without medium effect (same as the analytical model in Chapter III). (b) The effective densities are calculated from the different models.

Figure 5.2 shows the acoustic impedances of the plate and effective densities of the AMM with the water medium obtained from these three approaches. Based on the zero acoustic impedance, the first resonance frequency of the plate is around 3150 *Hz* (this

value is from the FEM model; in analytical model, the first resonance frequency of the plate is around 3350 *Hz*). Since the water medium provides a much more significant reaction pressure against plate vibration than does the air medium, the acoustic impedance of the plate increases (which is larger than zero; larger acoustic impedance means higher vibration resistance) to around 8900 *Hz* (the first resonance frequency for the case with the air medium) so that the lower first resonance frequency is expected.

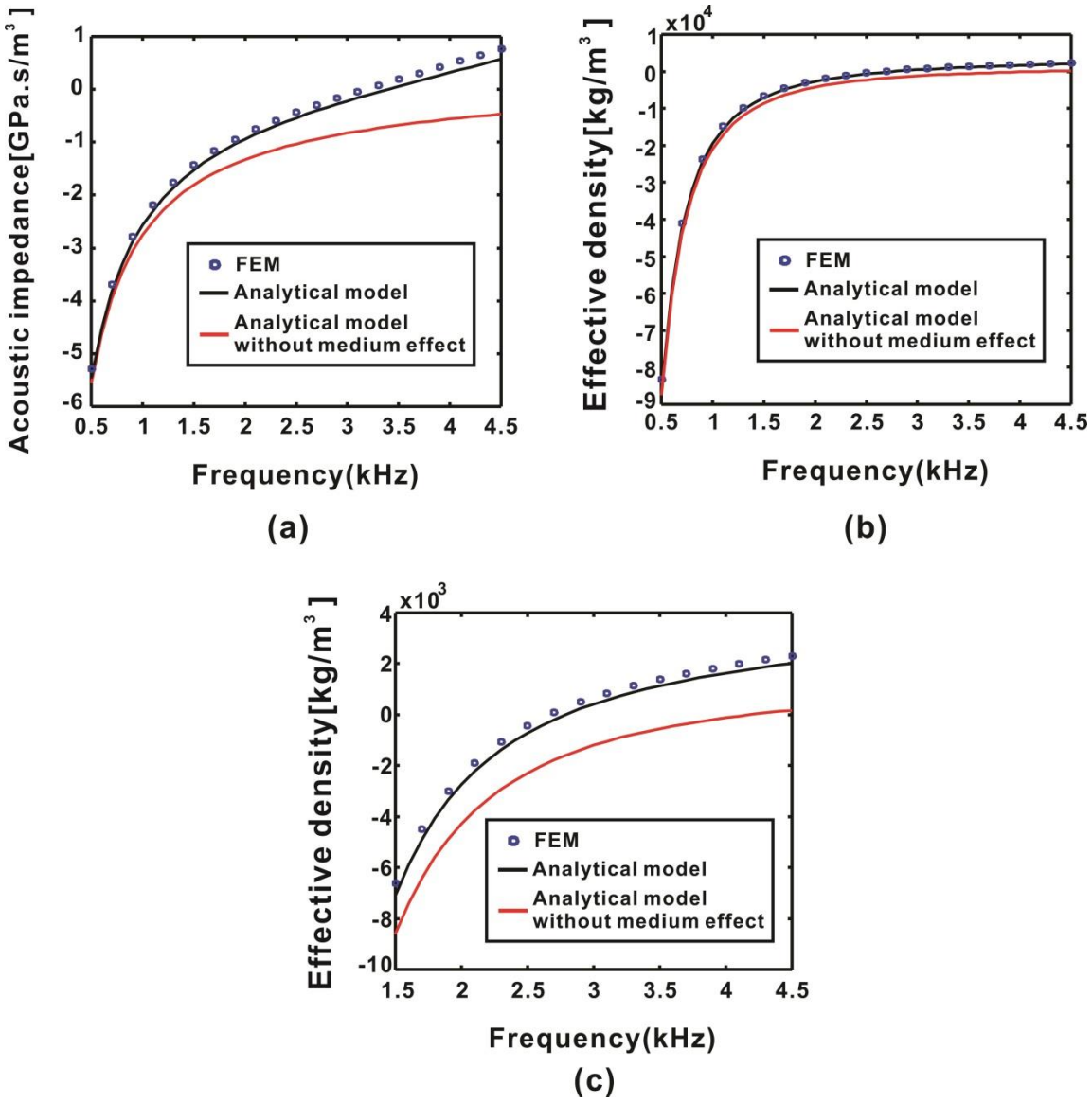

Figure 5.2. (a) The acoustic impedances of a fully-clamped square plate surrounded by the water medium from the FEM model, analytical model, and analytical model without the medium effect (same as the analytical model in chapter III). (b) The effective densities are calculated from the different models. (c) The effective densities are calculated from the different models, but with a narrower frequency range.

Fig. 5.2(c) plots the effective density of the AMM in a narrower frequency range and it more clearly shows that around the first resonance frequency (FEM result: 3150 *Hz*), the effective density is near the density of water, and the zero effective density is around 2650 *Hz* (FEM result), which is different from the case with the air medium. This phenomenon can be explained by Eq. (5.11). When the operating frequency approaches to the first resonance frequency of the plate, Z_{am} becomes to zero, and then the effective density is the density of the medium. If the medium is air, the effective density is close to zero (but is exactly equal to $\rho_{air} = 1.2 kg/m^3$) around the first resonance frequency of the plate.

5.3 Summary

This chapter demonstrates how the reaction pressure from the medium is taken into account in the structure of a plate-type AMM. After being validated by the FEM model results, this analytical model is capable of evaluating the effective densities of a plate-type AMM. Good agreements are found in the low-frequency region and frequency around the first resonance frequency of the plate. Since the heavy medium (water) resists the vibration of the plate, the first resonance frequency of the plate is significantly decreased. Moreover, since the density of water is not negligible, the corresponding frequency of the zero effective density is further decreased. This framework provides a robust method for designing the plate-type AMMs (without mass attached) that interaction with water. This extends the design regions from air to water.

Chapter VI

Conclusions and Future work

6.1 Conclusions

Analytical models for evaluating effective densities of the plate-type (or membrane-type) AMMs are derived and investigated in this dissertation. Starting from a square plate-type (or membrane-type) AMM, the acoustic impedance of a square, fully clamped plate (or membrane) is first obtained via an analytical model and an approximate model and then applied in the lumped model to evaluate the effective density of the AMM. The damping of a plate (or membrane) can be included in the analytical model. Good agreements between analytical and FEM results can be obtained for acoustic impedances, effective densities, and transmission coefficient.

Next, the meshless boundary method is applied to extend the capability of the analytical model to deal with arbitrarily shaped plate-type AMMs. The acoustic impedances and effective densities of AMMs with three different-shaped plates, i.e. a circle, a triangle, and a hexagon, are investigated to validate the analytical model. The damping of each plate can be considered, and good agreements for the circular and hexagonal cases are obtained. In the triangular case, a small discrepancy occurs in the low-frequency region, due to three corners, which cause inaccurate calculations of the average normal unit vectors for corners. Polygons with more sides, for example, the hexagon, can have more accurate results in low-frequency region.

Finally, the medium effect for plate-type AMMs is included by considering the reaction pressure from fluid medium in the equation of motion of a rectangular plate.

When the medium is water, a significant medium effect is observed in which the first resonance frequency of the plate is shifted down and the corresponding frequency of near-zero-effective density is further shifted down. Although the agreements (between results from analytical model and FEM model) in the case of air are better than in the case with water, the results for case with water are still in a reasonable accurate range (about 200 *Hz* discrepancy for the first resonance frequency).

6.2 Future work

Based on derived analytical models, plate-type AMMs can be efficiently and accurately designed. Some future work needs to be conducted.

First, utilize derived models to design plate-type AMMs. Second, the current analytical model assumes the waveguide is sound hard boundary and rigid, so the out-of-plane vibration of waveguide is ignored. If an application needs a large scale, the whole structure may vibrate as a plate and then the vibration of waveguides need to be considered. Third, these derived models are currently for 1-D AMMs only, but can be extended to the 2D case, which is suitable for the design of 2D AMMs, e.g. complimentary metamaterials (CMMs) [5].

BIBLIOGRAPHY

[1] F. Bongard, H. Lissek, and J. R. Mosig, "Acoustic transmission line metamaterial with negative/zero/positive refractive index," *Phys. Rev. B*, vol. 82, no. 9, p. 094306, Sep. 2010.

[2] G. Ma, "Membrane-type Acoustic Metamaterials," The Hong Kong University of Science and Technology, 2012.

[3] Z. Yang, J. Mei, M. Yang, N. H. Chan, and P. Sheng, "Membrane-Type Acoustic Metamaterial with Negative Dynamic Mass," *Phys. Rev. Lett.*, vol. 101, no. 20, p. 204301, Nov. 2008.

[4] G. Ma, M. Yang, S. Xiao, Z. Yang, and P. Sheng, "Acoustic metasurface with hybrid resonances," *Nat. Mater.*, vol. 13, pp. 873–878, 2014.

[5] C. Shen, J. Xu, N. X. Fang, and Y. Jing, "Anisotropic Complementary Acoustic Metamaterial for Canceling out Aberrating Layers," *Phys. Rev. X*, vol. 4, no. 4, p. 041033, Nov. 2014.

[6] B. I. Popa and S. a Cummer, "Non-reciprocal and highly nonlinear active acoustic metamaterials.," *Nat. Commun.*, vol. 5, p. 3398, Jan. 2014.

[7] V. G. Veselago, "The electrodynamics of substances with simultaneously negative values of the dielectric constant and the magnetic permeability," *Sov. Phys. Uspekhi*, vol. 10, no. 4, pp. 517–526, 1968.

[8] J. B. Pendry, A. J. Holden, D. J. Robbins, and W. J. Stewart, "Magnetism from Conductors and Enhanced Nonlinear Phenomena," *IEEE*, vol. 47, no. 11, pp. 2075–2084, 1999.

[9] J. B. Pendry, "Negative refraction makes a perfect lens," *Phys. Rev. Lett.*, vol. 85, no. 18, pp. 3966–9, Oct. 2000.

[10] D. Schurig, J. J. Mock, B. J. Justice, S. A. Cummer, J. B. Pendry, A. F. Starr, and D. R. Smith, "Metamaterial Electromagnetic Cloak at Microwave Frequencies," *Science (80-.).*, vol. 314, pp. 977–980, 2006.

[11] Y. Cui, K. H. Fung, J. Xu, Y. Jin, S. He, and N. X. Fang, "Ultrabroadband Light Absorption by a Sawtooth Anisotropic Metamaterial Slab," *Nano Lett.*, vol. 12, pp. 1443–1447, 2012.

[12] Z. Liu, X. Zhang, Y. Mao, Y. Y. Zhu, Z. Yang, C. T. Chan, and N. Series, "Locally Resonant Sonic Materials," *Science (80-.).*, vol. 289, no. 5485, pp. 1734–1736, 2000.

[13] N. Fang, D. Xi, J. Xu, M. Ambati, W. Srituravanich, C. Sun, and X. Zhang, "Ultrasonic metamaterials with negative modulus.," *Nat. Mater.*, vol. 5, no. 6, pp. 452–456, Jun. 2006.

[14] G. Ma and P. Sheng, "Acoustic metamaterials : From local resonances to broad horizons," *Sci. Adv.*, vol. 2, no. 2, p. e1501595, 2016.

[15] Y. Wu, Y. Lai, and Z.-Q. Zhang, "Elastic Metamaterials with Simultaneously Negative Effective Shear Modulus and Mass Density," *Phys. Rev. Lett.*, vol. 107, no. 10, p. 105506, Sep. 2011.

[16] R. Zhu, X. N. Liu, G. K. Hu, C. T. Sun, and G. L. Huang, "Negative refraction of elastic waves at the deep-subwavelength scale in a single-phase metamaterial.," *Nat. Commun.*, vol. 5, p. 5510, Jan. 2014.

[17] R. Zhu, X. N. Liu, G. K. Hu, F. G. Yuan, and G. L. Huang, "Microstructural designs of plate-type elastic metamaterial and their potential applications: a review," *Int. J. Smart Nano Mater.*, vol. 6, no. 1, pp. 14–40, Mar. 2015.

[18] S. a. Cummer, J. Christensen, and A. Alù, "Controlling sound with acoustic metamaterials," *Nat. Rev. Mater.*, vol. 1, no. 3, p. 16001, Feb. 2016.

[19] T.-Y. Huang, C. Shen, and Y. Jing, "Membrane- and plate-type acoustic metamaterials.," *J. Acoust. Soc. Am.*, vol. 139, no. 6, pp. 3240–3250, Jun. 2016.

[20] Z. Liu, X. Zhang, Y. Mao, Y. Zhu, and Z. Yang, "Locally resonant sonic materials," *Science (80-.).*, vol. 289, pp. 1734–1736, 2000.

[21] Z. Yang, J. Mei, M. Yang, N. Chan, and P. Sheng, "Membrane-Type Acoustic Metamaterial with Negative Dynamic Mass," *Phys. Rev. Lett.*, vol. 101, no. 20, p. 204301, Nov. 2008.

[22] C. J. Naify, C. M. Chang, G. McKnight, and S. Nutt, "Transmission loss of membrane-type acoustic metamaterials with coaxial ring masses," *J. Appl. Phys.*, vol. 110, no. 12, p. 124903, 2011.

[23] Z. Yang, H. M. Dai, N. H. Chan, G. C. Ma, and P. Sheng, "Acoustic metamaterial panels for sound attenuation in the 50–1000 Hz regime," *Appl. Phys. Lett.*, vol. 96, no. 4, p. 041906, 2010.

[24] C. J. Naify, C. M. Chang, G. McKnight, and S. Nutt, "Transmission loss and dynamic response of membrane-type locally resonant acoustic metamaterials," *J. Appl. Phys.*, vol. 108, no. 11, p. 114905, 2010.

[25] C. J. Naify, C. M. Chang, G. McKnight, F. Scheulen, and S. Nutt, “Membrane-type metamaterials: Transmission loss of multi-celled arrays,” *J. Appl. Phys.*, vol. 109, no. 10, p. 104902, 2011.

[26] S. H. Lee, C. M. Park, Y. M. Seo, Z. G. Wang, and C. K. Kim, “Acoustic metamaterial with negative density,” *Phys. Lett. A*, vol. 373, no. 48, pp. 4464–4469, Dec. 2009.

[27] S. Yao, X. Zhou, and G. Hu, “Investigation of the negative-mass behaviors occurring below a cut-off frequency,” *New J. Phys.*, vol. 12, no. 10, p. 103025, Oct. 2010.

[28] T.-Y. Huang, C. Shen, and Y. Jing, “On the evaluation of effective density for plate- and membrane-type acoustic metamaterials without mass attached.,” *J. Acoust. Soc. Am.*, vol. 140, no. 2, p. 908, Aug. 2016.

[29] C. Shen, Y. Xie, N. Sui, W. Wang, S. a. Cummer, and Y. Jing, “Broadband Acoustic Hyperbolic Metamaterial,” *Phys. Rev. Lett.*, vol. 115, no. 25, p. 254301, Dec. 2015.

[30] N. Sui, X. Yan, T.-Y. Huang, J. Xu, F.-G. Yuan, and Y. Jing, “A lightweight yet sound-proof honeycomb acoustic metamaterial,” *Appl. Phys. Lett.*, vol. 106, no. 17, p. 171905, Apr. 2015.

[31] X. Zhou and G. Hu, “Superlensing effect of an anisotropic metamaterial slab with near-zero dynamic mass,” *Appl. Phys. Lett.*, vol. 98, no. 26, p. 263510, 2011.

[32] X. Xu, P. Li, X. Zhou, and G. Hu, “Experimental study on acoustic subwavelength imaging based on zero-mass metamaterials,” *EPL (Europhysics Lett.*, vol. 109, no. 2, p. 28001, Jan. 2015.

[33] P. Li, X. Chen, X. Zhou, G. Hu, and P. Xiang, “Acoustic cloak constructed with thin-plate metamaterials,” *Int. J. Smart Nano Mater.*, vol. 6, no. 1, pp. 73–83, Mar. 2015.

[34] Y. Jing, J. Xu, and N. X. Fang, “Numerical study of a near-zero-index acoustic metamaterial,” *Phys. Lett. A*, vol. 376, no. 45, pp. 2834–2837, Oct. 2012.

[35] R. Fleury and A. Alù, “Extraordinary Sound Transmission through Density-Near-Zero Ultranarrow Channels,” *Phys. Rev. Lett.*, vol. 111, no. 5, p. 055501, Jul. 2013.

[36] P. Sheng, X. X. Zhang, Z. Liu, and C. T. Chan, “Locally resonant sonic materials,” *Phys. B Condens. Matter*, vol. 338, no. 1–4, pp. 201–205, Oct. 2003.

[37] L. Zigoneanu, B. Popa, and S. A. Cummer, “Three-dimensional broadband omnidirectional acoustic ground cloak,” *Nat. Mater.*, vol. 13, pp. 352–355, 2014.

[38] B.-I. Popa, L. Zigoneanu, and S. a. Cummer, “Experimental Acoustic Ground Cloak in Air,” *Phys. Rev. Lett.*, vol. 106, no. 25, p. 253901, Jun. 2011.

[39] Z. Liang and J. Li, “Extreme Acoustic Metamaterial by Coiling Up Space,” *Phys. Rev. Lett.*, vol. 108, no. 11, p. 114301, Mar. 2012.

[40] Y. Xie, B. I. Popa, L. Zigoneanu, and S. A. Cummer, “Measurement of a Broadband Negative Index with Space-Coiling Acoustic Metamaterials,” *Phys. Rev. Lett.*, vol. 110, no. 17, p. 175501, Apr. 2013.

[41] Y. Li, B. Liang, X. Tao, X. Zhu, X. Zou, and J. Cheng, “Acoustic focusing by coiling up space,” *Appl. Phys. Lett.*, vol. 101, no. 23, p. 233508, 2012.

[42] Z. Liang, T. Feng, S. Lok, F. Liu, K. B. Ng, C. H. Chan, J. Wang, S. Han, S. Lee, and J. Li, “Space-coiling metamaterials with double negativity and conical dispersion.,” *Sci. Rep.*, vol. 3, p. 1614, Jan. 2013.

[43] Y. Li, B. Liang, Z. Gu, X. Zou, and J. Cheng, “Reflected wavefront manipulation based on ultrathin planar acoustic metasurfaces.,” *Sci. Rep.*, vol. 3, p. 2546, Jan. 2013.

[44] Y. Xie, W. Wang, H. Chen, A. Konneker, B.-I. Popa, and S. a Cummer, “Wavefront modulation and subwavelength diffractive acoustics with an acoustic metasurface.,” *Nat. Commun.*, vol. 5, p. 5553, Jan. 2014.

[45] C. M. Park, J. J. Park, S. H. Lee, Y. M. Seo, C. K. Kim, and S. H. Lee, “Amplification of Acoustic Evanescent Waves Using Metamaterial Slabs,” *Phys. Rev. Lett.*, vol. 107, no. 19, p. 194301, Nov. 2011.

[46] M. Badreddine Assouar, M. Senesi, M. Oudich, M. Ruzzene, and Z. Hou, “Broadband plate-type acoustic metamaterial for low-frequency sound attenuation,” *Appl. Phys. Lett.*, vol. 101, no. 17, p. 173505, 2012.

[47] M. Badreddine Assouar and M. Oudich, “Enlargement of a locally resonant sonic band gap by using double-sides stubbed phononic plates,” *Appl. Phys. Lett.*, vol. 100, no. 12, p. 123506, 2012.

[48] M. Oudich, B. Djafari-Rouhani, Y. Pennec, M. B. Assouar, and B. Bonello, “Negative effective mass density of acoustic metamaterial plate decorated with low frequency resonant pillars,” *J. Appl. Phys.*, vol. 116, no. 18, p. 184504, Nov. 2014.

[49] P. Jiang, X.-P. Wang, T.-N. Chen, and J. Zhu, “Band gap and defect state engineering in a multi-stub phononic crystal plate,” *J. Appl. Phys.*, vol. 117, no. 15, p. 154301, Apr. 2015.

[50] Y. Li, T. Chen, X. Wang, Y. Xi, and Q. Liang, “Enlargement of locally resonant sonic band gap by using composite plate-type acoustic metamaterial,” *Phys. Lett. A*, vol. 379, no. 5, pp. 412–416, Feb. 2015.

[51] S. Yao, X. Zhou, and G. Hu, “Investigation of the negative-mass behaviors occurring below a cut-off frequency,” *New J. Phys.*, vol. 12, p. 103025, 2010.

[52] Y. Chen, G. Huang, X. Zhou, G. Hu, and C. T. Sun, “Analytical coupled vibroacoustic modeling of membrane-type acoustic metamaterials: membrane model.,” *J. Acoust. Soc. Am.*, vol. 136, no. 3, p. 969, Sep. 2014.

[53] Y. Chen, G. Huang, X. Zhou, G. Hu, and C. T. Sun, “Analytical coupled vibroacoustic modeling of membrane-type acoustic metamaterials: Plate model,” *J. Acoust. Soc. Am.*, vol. 136, no. 6, pp. 2926–2934, 2014.

[54] S. Yao, X. Zhou, and G. Hu, “Experimental study on negative effective mass in a 1D mass–spring system,” *New J. Phys.*, vol. 10, no. 4, p. 043020, Apr. 2008.

[55] C. J. Naify and S. R. Nutt, “Scaling of membrane-type locally resonant acoustic metamaterial arrays,” *J. Acoust. Soc. Am.*, vol. 132, no. May, 2012.

[56] Y. Zhang, J. Wen, H. Zhao, D. Yu, L. Cai, and X. Wen, “Sound insulation property of membrane-type acoustic metamaterials carrying different masses at adjacent cells,” *J. Appl. Phys.*, vol. 114, no. 6, p. 063515, 2013.

[57] Y. Zhang, J. Wen, Y. Xiao, X. Wen, and J. Wang, “Theoretical investigation of the sound attenuation of membrane-type acoustic metamaterials,” *Phys. Lett. A*, vol. 376, no. 17, pp. 1489–1494, Mar. 2012.

[58] F. Langfeldt, W. Gleine, and O. von Estorff, “Analytical model for low-frequency transmission loss calculation of membranes loaded with arbitrarily shaped masses,” *J. Sound Vib.*, vol. 349, pp. 315–329, Aug. 2015.

[59] H. Tian, X. Wang, and Y. Zhou, “Theoretical model and analytical approach for a circular membrane–ring structure of locally resonant acoustic metamaterial,” *Appl. Phys. A*, vol. 114, no. 3, pp. 985–990, Oct. 2013.

[60] J. Mei, G. Ma, M. Yang, Z. Yang, W. Wen, and P. Sheng, “Dark acoustic metamaterials as super absorbers for low-frequency sound.,” *Nat. Commun.*, vol. 3, p. 756, Jan. 2012.

[61] M. Yang, Y. Li, C. Meng, C. Fu, J. Mei, Z. Yang, and P. Sheng, “Sound absorption by subwavelength membrane structures: A geometric perspective,” *Comptes Rendus Mécanique*, vol. In press, p. In press, Aug. 2015.

[62] M. Yang, C. Meng, C. Fu, Y. Li, Z. Yang, and P. Sheng, “Subwavelength total acoustic absorption with degenerate resonators,” *Appl. Phys. Lett.*, vol. 107, no. 10, p. 104104, Sep. 2015.

[63] M. Yang, G. Ma, Z. Yang, and P. Sheng, “Coupled Membranes with Doubly Negative Mass Density and Bulk Modulus,” *Phys. Rev. Lett.*, vol. 110, no. 13, p. 134301, Mar. 2013.

[64] F. Ma, J. H. Wu, M. Huang, W. Zhang, and S. Zhang, “A purely flexible lightweight membrane-type acoustic metamaterial,” *J. Phys. D. Appl. Phys.*, vol. 48, no. 17, p. 175105, May 2015.

[65] G. Ma, M. Yang, Z. Yang, and P. Sheng, “Low-frequency narrow-band acoustic filter with large orifice,” *Appl. Phys. Lett.*, vol. 103, no. 1, p. 011903, 2013.

[66] Y. Xiao, J. Wen, and X. Wen, “Sound transmission loss of metamaterial-based thin plates with multiple subwavelength arrays of attached resonators,” *J. Sound Vib.*, vol. 331, no. 25, pp. 5408–5423, Dec. 2012.

[67] P. Li, S. Yao, X. Zhou, G. Huang, and G. Hu, “Effective medium theory of thin-plate acoustic metamaterials.,” *J. Acoust. Soc. Am.*, vol. 135, no. 4, pp. 1844–52, Apr. 2014.

[68] M. Oudich, X. Zhou, and M. Badreddine Assouar, “General analytical approach for sound transmission loss analysis through a thick metamaterial plate,” *J. Appl. Phys.*, vol. 116, no. 19, p. 193509, Nov. 2014.

[69] V. E. Gusev and O. B. Wright, “Double-negative flexural acoustic metamaterial,” *New J. Phys.*, vol. 16, no. 12, p. 123053, Dec. 2014.

[70] S. H. Lee, C. M. Park, Y. M. Seo, Z. G. Wang, and C. K. Kim, “Composite Acoustic Medium with Simultaneously Negative Density and Modulus,” *Phys. Rev. Lett.*, vol. 104, no. 5, p. 054301, Feb. 2010.

[71] C. Shen and Y. Jing, “Side branch-based acoustic metamaterials with a broad-band negative bulk modulus,” *Appl. Phys. A*, vol. 117, no. 4, pp. 1885–1891, Jul. 2014.

[72] S. H. Lee, C. M. Park, Y. M. Seo, Z. G. Wang, and C. K. Kim, “Acoustic metamaterial with negative modulus.,” *J. Phys. Condens. Matter*, vol. 21, no. 17, p. 175704, Apr. 2009.

[73] S. H. Lee, C. M. Park, Y. M. Seo, and C. K. Kim, “Reversed Doppler effect in double negative metamaterials,” *Phys. Rev. B*, vol. 81, no. 24, p. 241102, Jun. 2010.

[74] L. Fan, Z. Chen, Y. Deng, J. Ding, H. Ge, S. Zhang, Y. Yang, and H. Zhang, "Nonlinear effects in a metamaterial with double negativity," *Appl. Phys. Lett.*, vol. 105, no. 4, p. 041904, Jul. 2014.

[75] C. J. Naify, C. N. Layman, T. P. Martin, M. Nicholas, D. C. Calvo, and G. J. Orris, "Experimental realization of a variable index transmission line metamaterial as an acoustic leaky-wave antenna," *Appl. Phys. Lett.*, vol. 102, no. 20, p. 203508, 2013.

[76] L. Fan, S.-Y. Zhang, and H. Zhang, "Transmission Characteristics in Tubular Acoustic Metamaterials Studied with Fluid Impedance Theory," *Chinese Phys. Lett.*, vol. 28, no. 10, p. 104301, Oct. 2011.

[77] L. Fan, H. Ge, S. Zhang, and H. Zhang, "Research on pass band with negative phase velocity in tubular acoustic metamaterial," *J. Appl. Phys.*, vol. 112, no. 5, p. 053523, 2012.

[78] M. Ambati, N. Fang, C. Sun, and X. Zhang, "Surface resonant states and superlensing in acoustic metamaterials," *Phys. Rev. B*, vol. 75, no. 19, p. 195447, May 2007.

[79] J. J. Park, C. M. Park, K. J. B. Lee, and S. H. Lee, "Acoustic superlens using membrane-based metamaterials," *Appl. Phys. Lett.*, vol. 106, no. 5, p. 051901, Feb. 2015.

[80] A. Liu, X. Zhou, G. Huang, and G. Hu, "Super-resolution imaging by resonant tunneling in anisotropic acoustic metamaterials," *J. Acoust. Soc. Am.*, vol. 132, no. May, 2012.

[81] J. J. Park, K. J. B. Lee, O. B. Wright, M. K. Jung, and S. H. Lee, "Giant Acoustic Concentration by Extraordinary Transmission in Zero-Mass Metamaterials," *Phys. Rev. Lett.*, vol. 110, no. 24, p. 244302, Jun. 2013.

[82] Y. Gu, Y. Cheng, J. Wang, and X. Liu, "Controlling sound transmission with density-near-zero acoustic membrane network," *J. Appl. Phys.*, vol. 118, no. 2, p. 024505, Jul. 2015.

[83] N. R. Mahesh and P. Nair, "Design and analysis of an acoustic demultiplexer exploiting negative density, negative bulk modulus and extra-ordinary transmission of membrane-based acoustic metamaterial," *Appl. Phys. A*, vol. 116, no. 3, pp. 1495–1500, Feb. 2014.

[84] N. Cselyuszka, M. Sečujski, and V. Crnojević-Bengin, "Novel negative mass density resonant metamaterial unit cell," *Phys. Lett. A*, vol. 379, no. 1–2, pp. 33–36, Jan. 2015.

[85] S. Varanasi, J. S. Bolton, T. H. Siegmund, and R. J. Cipra, “The low frequency performance of metamaterial barriers based on cellular structures,” *Appl. Acoust.*, vol. 74, pp. 485–495, 2013.

[86] S. Yao, P. Li, X. Zhou, and G. Hu, “Sound reduction by metamaterial-based acoustic enclosure,” *AIP Adv.*, vol. 4, no. 12, p. 124306, Dec. 2014.

[87] Z. Liu, H. Zhang, S. Zhang, and L. Fan, “An acoustic dual filter in the audio frequencies with two local resonant systems,” *Appl. Phys. Lett.*, vol. 105, no. 5, p. 053501, Aug. 2014.

[88] L. Fan, Z. Chen, S. Zhang, J. Ding, X. Li, and H. Zhang, “An acoustic metamaterial composed of multi-layer membrane-coated perforated plates for low-frequency sound insulation,” *Appl. Phys. Lett.*, vol. 106, no. 15, p. 151908, Apr. 2015.

[89] a Baz, “The structure of an active acoustic metamaterial with tunable effective density,” *New J. Phys.*, vol. 11, p. 123010, Dec. 2009.

[90] A. M. Baz, “An Active Acoustic Metamaterial With Tunable Effective Density,” *J. Vib. Acoust.*, vol. 132, no. 4, p. 041011, 2010.

[91] W. Akl and a. Baz, “Multicell Active Acoustic Metamaterial With Programmable Effective Densities,” *J. Dyn. Syst. Meas. Control*, vol. 134, no. 6, p. 061001, 2012.

[92] W. Akl and a. Baz, “Multi-cell Active Acoustic Metamaterial with Programmable Bulk Modulus,” *J. Intell. Mater. Syst. Struct.*, vol. 21, no. 5, pp. 541–556, Jan. 2010.

[93] W. Akl and A. Baz, “Experimental characterization of active acoustic metamaterial cell with controllable dynamic density,” *J. Appl. Phys.*, vol. 112, no. 8, p. 084912, 2012.

[94] W. Akl and A. Baz, “Analysis and experimental demonstration of an active acoustic metamaterial cell,” *J. Appl. Phys.*, vol. 111, no. 4, p. 044505, 2012.

[95] B. I. Popa, L. Zigoneanu, and S. a. Cummer, “Tunable active acoustic metamaterials,” *Phys. Rev. B*, vol. 88, no. 2, p. 024303, Jul. 2013.

[96] B. I. Popa, D. Shinde, A. Konneker, and S. A. Cummer, “Active acoustic metamaterials reconfigurable in real-time,” *Phys. Rev. B*, vol. 91, p. 220303, Apr. 2015.

[97] H. Zhang, J. Wen, Y. Xiao, G. Wang, and X. Wen, “Sound transmission loss of metamaterial thin plates with periodic subwavelength arrays of shunted piezoelectric patches,” *J. Sound Vib.*, vol. 343, pp. 104–120, May 2015.

[98] W. Akl and A. Baz, “Stability analysis of active metamaterial with programmable bulk modulus,” *Smart Mater. Struct.*, vol. 20, p. 125010, 2011.

[99] W. Akl and A. Baz, “Active Acoustic Metamaterial With Simultaneously Programmable Density and Bulk Modulus,” *J. Vib. Acoust.*, vol. 135, no. 3, p. 031001, Mar. 2013.

[100] W. Akl and A. Elsabbagh, “Acoustic metamaterials with circular sector cavities and programmable densities,” *J. Acoust. Soc. Am.*, vol. 132, no. October 2012, pp. 2857–2865, 2012.

[101] X. Chen, X. Xu, S. Ai, H. Chen, Y. Pei, and X. Zhou, “Active acoustic metamaterials with tunable effective mass density by gradient magnetic fields,” *Appl. Phys. Lett.*, vol. 105, no. 7, p. 071913, Aug. 2014.

[102] S. Xiao, G. Ma, Y. Li, Z. Yang, and P. Sheng, “Active control of membrane-type acoustic metamaterial by electric field,” *Appl. Phys. Lett.*, vol. 106, no. 9, p. 091904, Mar. 2015.

[103] H. Lissek, “Electroacoustic metamaterials: achieving negative acoustic properties with shunt loudspeakers,” in *Proceedings of Meetings on Acoustics*, 2013, vol. 19.

[104] R. Fleury, D. Sounas, and A. Alù, “An invisible acoustic sensor based on parity-time symmetry.,” *Nat. Commun.*, vol. 6, p. 5905, Jan. 2015.

[105] S. Zhang, L. Yin, and N. Fang, “Focusing Ultrasound with an Acoustic Metamaterial Network,” *Phys. Rev. Lett.*, vol. 102, no. 19, p. 194301, May 2009.

[106] C.-C.Sung and J. T. Jan, “The response of and sound power radiated by a clamped rectangular plate,” *J. Sound Vib.*, vol. 207, no. 3, pp. 301–317, 1997.

[107] W.Leissa, *Vibration of plates*. Washington, D.C.: NASA, 1969, p. 61.

[108] Y. Cheng, J. Y. Xu, and X. J. Liu, “One-dimensional structured ultrasonic metamaterials with simultaneously negative dynamic density and modulus,” *Phys. Rev. B*, vol. 77, no. 4, p. 045134, Jan. 2008.

[109] S. H. Lee and O. B. Wright, “Origin of negative density and modulus in acoustic metamaterials,” *Phys. Rev. B*, vol. 93, no. 2, p. 024302, Jan. 2016.

[110] L. E. Kinsler, A. R. Frey, A. B. Coppens, and J. V. Sanders, *Fundamentals of acoustics*, 4th ed. Hoboken, NJ: John Wiley & Sons, Inc., 2000, pp. 92–94.

[111] J. T. Chen, I. L. Chen, K. H. Chen, Y. T. Lee, and Y. T. Yeh, “A meshless method for free vibration analysis of circular and rectangular clamped plates using radial basis function,” *Eng. Anal. Bound. Elem.*, vol. 28, no. 5, pp. 535–545, May 2004.

[112] S. W. Kang and J. M. Lee, “Free Vibration Analysis of Arbitrarily Shaped Plates With Clamped Edges Using Wave-Type Functions,” *J. Sound Vib.*, vol. 242, no. 1, pp. 9–26, Apr. 2001.

[113] Z. Skvor, *Vibrating Systems and their Equivalent Circuits*. 1991, p. 60.

[114] S. Zhang, C. Xia, and N. Fang, “Broadband Acoustic Cloak for Ultrasound Waves,” *Phys. Rev. Lett.*, vol. 106, no. 2, p. 024301, Jan. 2011.

[115] L. Maestrellod and A. Baylissd, “Coupling between plate vibration and acoustic radiation,” 1992.

[116] L. E. Kinsler, A. R. Frey, A. B. Coppens, and J. V. Sanders, *Fundamentals of Acoustics*. 2000, p. 256.